國 立 交 通 大 學

電信工程學系碩士班

碩士論文

基於軟體無線電之寬頻無線接取系統設計

Design of a Software Defined Radio Based Broadband Wireless Access System

研 究 生：葉舜文　　Student: Shuen-Wen Yeh

指導教授：李大嵩 博士　　Advisor: Dr. Ta-Sung Lee

中 華 民 國 九 十 五 年 六 月

基於軟體無線電之寬頻無線接取系統設計

Design of a Software Defined Radio Based Broadband Wireless Access System

研 究 生：葉舜文　　Student: Shuen-Wen Yeh

指導教授：李大嵩 博士　　Advisor: Dr. Ta-Sung Lee

國立交通大學

電信工程學系碩士班

碩士論文

A Thesis
Submitted to Department of Communication Engineering
College of Electrical Engineering and Computer Science
National Chiao Tung University
in Partial Fulfillment of the Requirements
for the Degree of
Master of Science
in
Communication Engineering
June 2006
Hsinchu, Taiwan, Republic of China

中 華 民 國 九 十 五 年 六 月

基於軟體無線電之寬頻無線接取系統設計

學生：葉舜文　　指導教授：李大嵩 博士

國立交通大學電信工程學系碩士班

摘要

寬頻無線網路即將給人們的生活帶來突破性的變化，不論在何時何地都能以高傳輸速率得到想獲取的資訊。WiMAX (Worldwide Interoperability for Microwave Access; 全球互通的微波存取)，目前已準備好成為新一代的寬頻無線接取技術並可提供固定式及移動式的網路服務。新興的 IEEE 802.16-2005 規格為了在不同的無線傳輸服務達到最佳化，整合了三種空中傳輸介面：單載波模式(Single Carrier, SC)、正交分頻多工模式(Orthogonal Frequency Division Multiplexing, OFDM)及正交分頻多重接取模式(Orthogonal Frequency Division Multiple Access, OFDMA)。在本論文中，吾人將探討 SC-OFDM-OFDMA 三模收發機之共同設計；藉由軟體定義無線電(Software Defined Radio, SDR)概念的引入，吾人設計之收發機架構可在單一平台上有效支援 IEEE 802.16-2005 所定義的三種空中傳輸介面。吾人將探討此共同設計所需之通道估測、時序同步及載波頻率估測等方法；具體而言，吾人將提出共同設計之時序及載波頻率飄移估測法。為了進一步提高系統傳輸的距離及可靠性，吾人在此架構中利用 IEEE 802.16-2005 所定義的多根天線傳輸技術，如時空編碼(Space-Time Coding, STC)及適應性天線系統(Adaptive Antenna System, AAS)等。最後，吾人將藉由電腦模擬驗證所提出之共同設計之 SC-OFDM-OFDMA 收發機架構，在無線通訊環境中具有可靠的傳輸效能，並展示出多根天線傳輸技術可帶來效能的改善。

Design of a Software Defined Radio Based Broadband Wireless Access System

Student: Shuen-Wen Yeh Advisor: Dr. Ta-Sung Lee

Department of Communication Engineering

National Chiao Tung University

Abstract

Broadband wireless will revolutionize people's lives by enabling a high-speed connection directly to the information they need, whenever and wherever they need it. WiMAX (Worldwide Interoperability for Microwave Access) is poised to become a key technical underpinning of fixed, portable and mobile data networks. It's the development of the emerging IEEE 802.16 standard that integrates Single Carrier (SC), Orthogonal Frequency Division Multiplexing (OFDM) and Orthogonal Frequency Division Multiple Access (OFDMA) for the optimization of different wireless data services. In this thesis, we investigate the joint design of SC-OFDM-OFDMA transceivers on a single platform via the concept of Software Defined Radio (SDR) to support various air-interface standards specified by IEEE 802.16-2005. In this way, the system possesses as many common components as possible for these three modes, and the transmitter and receiver can be switched among the three modes via SDR operation. Synchronization schemes for the SDR system are also investigated in this thesis. In particular, we propose a joint design of timing and frequency synchronization algorithm with lower computational complexity. In order to increase the range and reliability of the system, the use of multiple-antenna techniques such as Space-Time Coding (STC)

and Adaptive Antenna Systems (AAS) in IEEE 802.16-2005 is also considered and verified to exhibit improved performance. Finally, we evaluate the performance of the joint design of SC-OFDM-OFDMA SDR system and confirm that it works reliably under the three modes.

Acknowledgement

I would like to express my deepest gratitude to my advisor, Dr. Ta-Sung Lee, for his enthusiastic guidance and great patience. I also wish to thank my friends for their encouragement and help. Finally, I would like to show my sincere thanks to my parents for their inspiration and love.

Contents

List of Figures

List of Tables

Acronym Glossary

AAS	adaptive antenna system
AMC	adaptive modulation and coding
BER	bit error rate
BPSK	binary phase shift keying
BS	base station
BW	bandwidth
BWA	broadband wireless access
CC	convolutional code
CCIR	co-channel interference rejection
CINR	carrier-to-interference-and-noise ratio
CP	cyclic prefix
DL	downlink
DLFP	downlink frame prefix
FDD	frequency division duplex
FEC	forward error correction
FFT	fast fourier transform
FUSC	full usage of subchannels
ICI	inter carrier interference
IE	information element
IEEE	institute of electrical and electronics engineers

IFFT	inverse fast fourier transform
ISI	inter symbol interference
ITU	international telecommunications union
LOS	line-of-sight
MAC	medium access control
MIMO	multiple input multiple output
NLOS	non-line-of-sight
OFDM	orthogonal frequency division multiplexing
OFDMA	orthogonal frequency division multiple access
PHY	physical layer
PRBS	pseudo-random binary sequence
PUSC	partial usage of subchannels
QAM	quadrature amplitude modulation
QoS	quality of service
QPSK	quadrature phase shift keying
RS	reed solomon
Rx	receiver
SC	single carrier
SDR	software defined radio
SNR	signal-to-noise ratio
SOFDMA	scalable orthogonal frequency division multiple access
SP	short preamble
SS	subscriber station
STC	space time coding
TDD	time division duplex
TDMA	time division multiple access

Tx	transmitter
UL	uplink
WiMAX	worldwide interoperability for microwave access

Notations

N_t	number of transmit antennas
M	number of data subcarriers
L	maximum length of the channel
H	channel frequency response
l_{LP}	known long preamble
ν	correlation window size
Δf	frequency offset between the transmitter and receiver (unit in Hz)
Δf_r	residual frequency offset (unit in Hz)
Ψ	delay correlation outputs
Ψ_i	timing acquisition metric
q_s	phase estimator
N	FFT size
m	modulation order
c	convolutional code rate
N_{SC}	number of subchannels allocated
T_{FFT}	symbol duration of the useful part of the received signal
T_{samp}	sampling time
E_b	bit energy
E_s	symbol energy

Chapter 1

Introduction

Wireless communication systems have been in use for quite a long time. Many standards are available based on which these devices communicate, but the present standards fail to provide sufficient data rate, when the user is moving at high speed. Broadband wireless access is an appealing way to provide flexible and easily-deployable solution for high speed communications. In view of this requirement for future mobile wireless communication systems, the 802.16 standard has been proposed by Institute of Electrical and Electronic Engineers (IEEE) [1], [2].

The WiMAX (Worldwide Interoperability for Microwave Access) Forum is committed to providing optimized solutions for fixed, nomadic, portable and mobile broadband wireless access. Two versions of WiMAX address the demand for these different types of access:

• **IEEE 802.16-2004 (802.16d):** This is based on the 802.16-2004 version of the IEEE 802.16 standard. It uses Orthogonal Frequency Division Multiplexing (OFDM) and supports fixed and nomadic access in Line of Sight (LOS) and Non Line of Sight (NLOS) environments. The initial WiMAX Forum profiles are in the 3.5 GHz and 5.8 GHz frequency bands. The first certified products are expected by the end of 2005.

• **IEEE 802.16-2005 (802.16e):** Optimized for dynamic mobile radio channels,

this version is based on the IEEE 802.16-2005 amendment and provides support for handoffs and roaming. It uses Scalable Orthogonal Frequency Division Multiplexing Access (SOFDMA), a multi-carrier modulation technique that uses sub-channelization. Service providers that deploy IEEE 802.16-2005 can also use the network to provide fixed service. The WiMAX Forum has not yet announced the frequency bands for the IEEE 802.16-2005 profiles, but 2.3 GHz and 2.5 GHz are the most likely initial candidates.

Broadband wireless communications have a wide bandwidth, which may exceed the coherence bandwidth of the channel. In this case, the fading is likely to be frequency selective, and an equalizer must be used to mitigate the inter symbol interference (ISI). OFDM is a very effective method for combating the frequency selective fading as shown in Figure 1.1. It divides the transmission bandwidth into many narrow band subcarriers and uses these subcarriers to transmit signals in parallel. Since the bandwidth of each subcarrier is smaller than the coherence bandwidth of a multipath fading channel, from the viewpoint of each subcarrier the channel can be regarded as frequency-nonselective. Therefore, OFDM seems to be a good solution for overcoming the ISI due to multipath propagation.

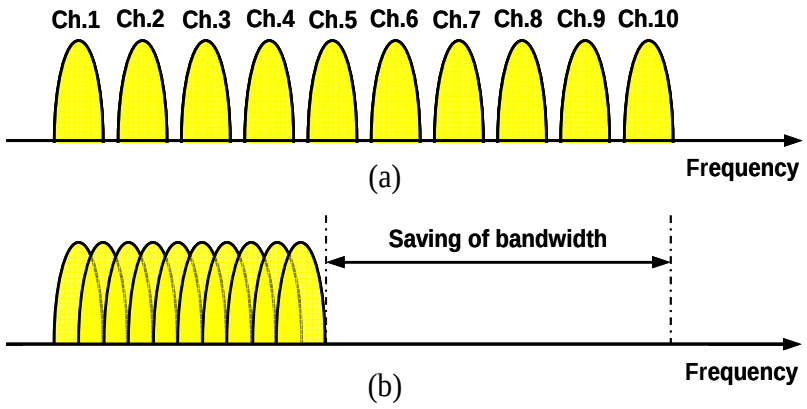

Figure 1.1: (a) Conventional multicarrier technique (b) Orthogonal multicarrier modulation technique

Since early 1980, a lot of standards of communication systems have been proposed due to an exponential growing of demands for communication. The industrial competition among Asia, Europe, and North America presents a difficult path toward a unique standard for future mobile systems. This therefore prompts the development of the Software Defined Radio (SDR) concept as a potential practical solution, with a flexible transmitter/receiver architecture, controlled or programmable by software.

Broadband, multi-carrier and SDR mobile wireless network infrastructure is directly applicable to the emerging IEEE 802.16 technologies, particularly the IEEE 802.16-2005 mobile high-speed data requirements. OFDM waveforms, as used in the IEEE 802.16 technology, can be very efficiently implemented using Fast Fourier Transform (FFT) techniques to provide significant architecture advantages.

This motivates us to investigate the jointly designed scheme for the Single carrier (SC), OFDM and OFDMA transceivers under the SDR system architecture, which is the principle part of this thesis. We aim to combine the transmitter and receiver architectures of the three transmission techniques, SC, OFDM and OFDMA (based on IEEE 802.16-2005 standard), as much as possible under the SDR system architecture. In this way, the transceiver possesses as many common components as possible for SC, OFDM and OFDMA modes, and the transmission mode of the combined transceiver architecture can be switched among the three modes via the concept of SDR operation.

Synchronization, channel estimation schemes, and phase estimation scheme for the jointly designed transceiver are also investigated in this thesis. In particular, we propose a jointly designed timing offset and frequency offset estimation scheme with low computational complexity. The jointly designed timing offset and frequency offset estimation scheme is developed based on the common delay correlation outputs. The computational complexity of the proposed synchronization scheme is lower than that of the conventional scheme because the proposed scheme can reuse the same delay

correlation outputs.

The rest of this thesis is organized as follows. In Chapter 2, an overview of WiMAX system is given. The transmit techniques such as Space-Time Coding (STC) and Adaptive Antenna System (AAS) are also introduced. In Chapter 3, channel estimation and joint design of timing offset and frequency offset estimation scheme are introduced. The phase estimation and the residual frequency offset estimation are also described, and then computer simulations show that the frequency offset can be corrected more accurately after compensating the residual frequency offset. In Chapter 4, we propose a SC-OFDM-OFDMA SDR system to support the various air-interface standards specified by IEEE 802.16-2005 on a single SDR platform. Some receiver functional blocks will be modified to adapt to different modes. In Chapter 5, we conclude this thesis.

Chapter 2

Overview of WiMAX System

WiMAX is a broadband wireless technology that supports fixed, nomadic, portable and mobile access. To meet the requirements of different types of access, two versions of WiMAX have been defined. The first is based on IEEE 802.16-2004 and is optimized for fixed and nomadic access. The second version is designed to support portability and mobility, and will be based on the IEEE 802.16-2005 amendment to the standard. In this chapter, an overview of WiMAX PHY will be given first. As with IEEE 802.16-2004, IEEE 802.16-2005 will incorporate previous versions of the standard and add support for fixed and mobile access. In this chapter, we will focus on the physical layer of IEEE 802.16-2005 and provide a detail introduction of Scalable OFDMA (SOFDMA) technology. Finally, the transmit techniques such as STC and AAS adopted in the system will be introduced.

2.1 Physical Layer Description

Worldwide Interoperability of Microwave Access (WiMAX) is a technology based on the IEEE 802.16 specifications to enable the delivery of last mile wireless broadband access as an alternative to cable and DSL. WiMAX will provide fixed, nomadic, and portable mobile wireless broadband connectivity without the requirement for direct line-of-sight with a base station. WiMAX provides metropolitan area network connectivity at speeds of up to 75 Mb/sec. WiMAX systems can be used to transmit signal as far as 30 miles. However, on the average a WiMAX base-station installation will likely cover between three to five miles [3].

WiMAX covers both LOS and NLOS applications in the 2-66 GHz frequencies. The PHY layer contains several forms of modulation and multiplexing to support different frequency range and application. Data rates determined by exact modulation and encoding schemes are shown in Table 2.1. The IEEE 802.16 standard was originally written to support several physical medium interfaces and it is expected that it will continue to develop and extend to support other PHY specifications. Hence, the modular nature of the standard is helpful in this aspect. For example, the first version of the standard only supported single carrier modulation. Since that time, OFDM has been added [4].

Table 2.1: Data rate for different modulations and code rates under different bandwidths

Bandwidth (MHz)	Raw bit rate (Mb/s)		
	QPSK, CC3/4	**16QAM, CC3/4**	**64QAM, CC3/4**
6	7.5	15	22.5
7	8.7	17.5	26.1
20	24.4	48.8	73.2

In IEEE 802.16-2004, its applications are focused on fixed and nomadic applications in the 2-11 GHz. Two multi-carrier modulation techniques are supported in 802.16-2004: OFDM with 256 carriers and OFDMA with 2048 carriers.

In December 2002, Task Group e was created to improve support for combined fixed and mobile operation in frequencies below 6 GHz. Work on the IEEE 802.16-2005 amendment is completion and has been approved by the IEEE. The new version of the standard introduces support for SOFDMA which allows for a variable number of carriers, in addition to the previously-defined OFDM and OFDMA modes. The carrier allocation in OFDMA modes is designed to minimize the effect of the interference on user devices with omni-directional antennas. Furthermore, IEEE 802.16-2005 offers improved support for Multiple Input Multiple Output (MIMO) and AAS, as well as hard and soft handoffs. It also has improved power-saving capabilities for mobile devices and more extensive security features. Both OFDM- and OFDMA-based products can take advantage of the newly added capabilities [5].

In the following sections, we will introduce the main block diagrams of the transmitter architecture. We put emphasis on OFDM mode and OFDMA mode rather than on SC mode. OFDM mode and OFDMA mode have many common blocks such as randomizer, FEC, interleaver, and modulator, so we will introduce them together and point the differences if necessary.

2.1.1 Randomizer

The randomization is performed on each burst of data on the DL and UL, which means that for each allocation of a data block, the randomizer shall be used independently. For RS and CC encoded data, padding will be added to the end of the transmission block, up to the amount of data allocated minus one byte, which shall be

reserved for the introduction of a 0x00 tail byte by the FEC. The PRBS generator shall be $1+X^{14}+X^{15}$ as shown in Figure 2.1. Each data byte to be transmitted shall enter sequentially into the randomizer. Preambles are not randomized.

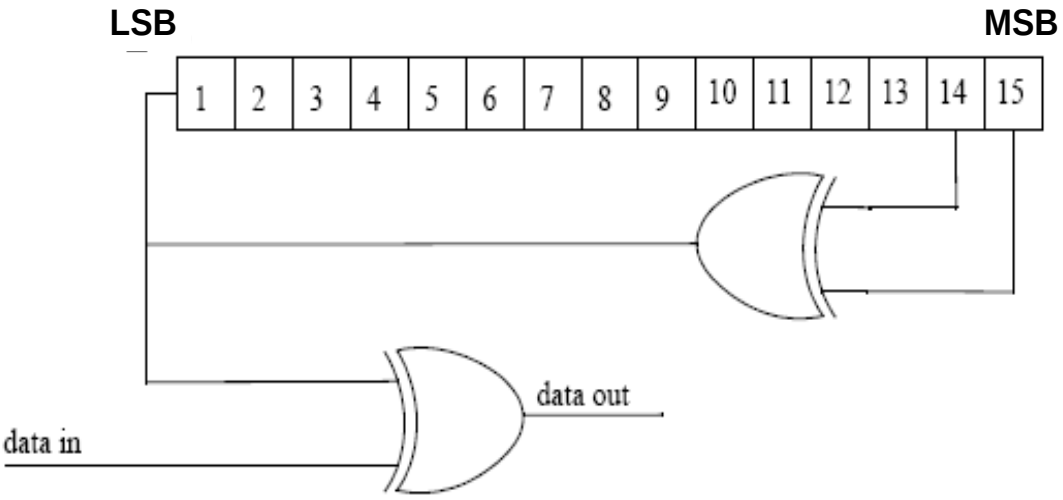

Figure 2.1: PRBS generator for randomizer

On the downlink, the randomizer shall be re-initialized at the start of each frame. In OFDM mode, the randomizer shall be re-initialized with the sequence: 100101010000000. At the start of subsequent bursts, the randomizer shall be initialized with the vector shown in Figure 2.2. The frame number used for initialization refers to the frame in which the DL burst is transmitted. In OFDMA mode, the randomizer shall be initialized with the vector shown in Figure 2.3. The subchannel offset used for initialization refers to the allocated subchannels in which the DL burst is transmitted.

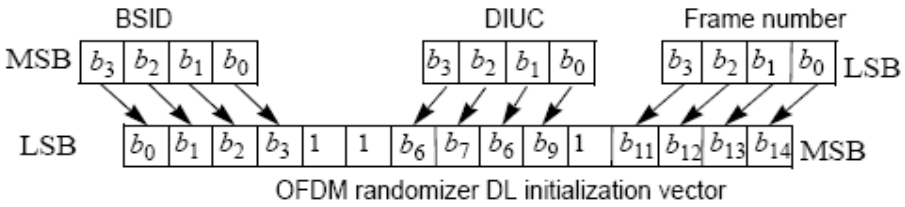

Figure 2.2: OFDM randomizer DL initialization vector

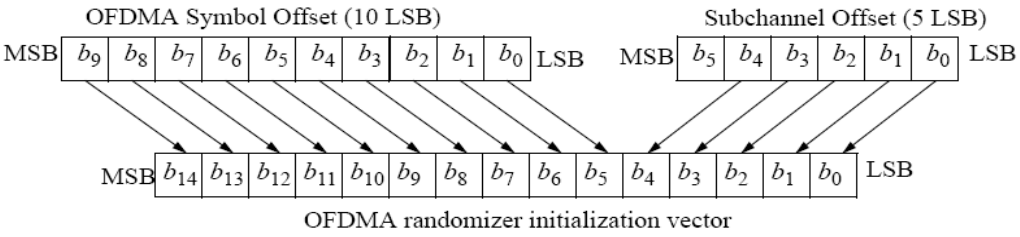

Figure 2.3: OFDMA randomizer DL initialization vector

2.1.2 Forward Error Correction

In OFDM mode, the encoding is performed by first passing the data in block format through RS encoder and then passing it through a convolutional encoder. A single 0x00 tail byte is appended to the end of each burst after randomization. The Reed-Solomon encoding shall be derived from a systematic RS (N = 255, K = 239, T = 8) code using GF(2^8), where N is the number of overall bytes after encoding, K is the number of overall bytes before encoding, and T is the number of data bytes that can be corrected.

Each RS block is encoded by the binary convolutional encoder, which shall have native rate of 1/2, a constraint length equal to 7, and shall use the generator depicted in Figure 2.4. Puncturing patterns and serialization order that shall be used to realize different code rates are defined in Table 2.2. The RS-CC rate 1/2 shall always be used to as the coding mode when requesting access to the network. Table 2.3 gives the block sizes and the code rates used for the different modulations. In the case of BPSK modulation, the RS encoder shall be bypassed.

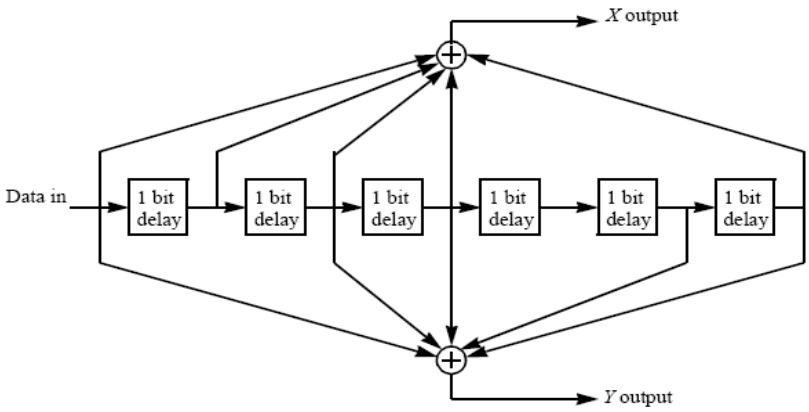

Figure 2.4: Convolutional encoder

Table 2.2: Puncturing patterns and serialization orders to realize different code rates

	Code rates			
Rate	1/2	2/3	3/4	5/6
d_{free}	10	6	5	4
X	1	10	101	10101
Y	1	11	110	11010
XY	X_1Y_1	$X_1Y_1Y_2$	$X_1Y_1Y_2X_3$	$X_1Y_1Y_2X_3Y_4X_5$

Table 2.3: Uncoded block size for different modulations and code rates

Modulation	Uncoded block size (bytes)	Coded block size (bytes)	Overall coding rate	RS code	CC code rate
BPSK	12	24	1/2	(12,12,0)	1/2
QPSK	24	48	1/2	(32,24,4)	2/3
QPSK	36	48	3/4	(40,36,2)	5/6
16-QAM	48	96	1/2	(64,48,8)	2/3
16-QAM	72	96	3/4	(80,72,4)	5/6
64-QAM	96	144	2/3	(108,96,6)	3/4
64-QAM	108	144	3/4	(120,108,6)	5/6

In OFDMA mode, the encoding is performed by passing the data block through a convolutional encoder. Its convolutional encoder is the same as OFDM mode. The RS encoder shall be dismissed in OFDMA mode.

2.1.3 Interleaver

All encoded data bits shall be interleaved by a block interleaver with a block size corresponding to the number of coded bits over the allocated subchannels per OFDM symbol. The interleaver is defined by two step permutation. The first permutation ensures that adjacent coded bits are mapped onto nonadjacent subcarriers. The second permutation ensures that adjacent coded bits are mapped alternately onto less or more significant bits of the constellation, thus avoiding long runs of lowly reliable bits.

2.1.4 Modulator

After bit interleaving, the data are entered serially to the constellation mapper. For OFDM mode, BPSK, Gray-mapped QPSK, and 16QAM are mandatory. The constellations shall be normalized by multiplying the constellation point with the indicated factor *c* to achieve equal average power. The constellation-mapped data shall be subsequently modulated onto all allocated data subcarriers in order of increasing frequency offset index. For OFDMA mode, Gray-mapped QPSK, 16QAM, and 64QAM shall be supported. The constellation-mapped data shall be subsequently modulated onto all allocated data subcarriers and each subcarrier multiplied by the factor $2*(1/2-w_k)$ according the subcarrier index, *k*.

2.1.4.1 Pilot Modulation

Pilot subcarriers shall be inserted into each data burst in order to constitute the symbol and they shall be modulated according to their carrier location within the symbol. The PRBS generator depicted in Figure 2.5 shall be used to produce a sequence, w_k. The polynomial for the PRBS generator shall be $1+X^9+X^{11}$. For OFDM mode, each pilot is BPSK modulated and located at the fixed locations in each symbol. For OFDMA mode, each pilot shall be transmitted with a boosting of 2.5 dB over the average power of each data tone. The pilot subcarriers shall be modulated according to Equation (2.1):

$$\mathrm{Re}\{c_k\} = \frac{8}{3}\left(\frac{1}{2} - w_k\right) \quad \text{and} \quad \mathrm{Im}\{c_k\} = 0 \tag{2.1}$$

The pilot in DL preamble shall be modulated according to Equation (2.2):

$$\begin{aligned} \mathrm{Re}\{premablePilotsModulated\} &= 4\cdot\sqrt{2}\cdot\left(\frac{1}{2} - w_k\right) \\ \mathrm{Im}\{premablePilotsModulated\} &= 0 \end{aligned} \tag{2.2}$$

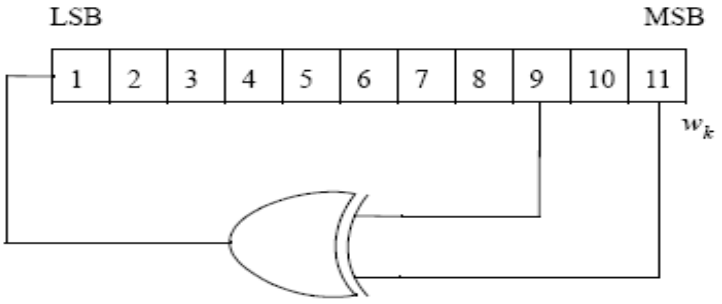

Figure 2.5: PRBS generator for pilot modulation

2.1.4.2 Preamble Structure

For OFDM mode, all preambles are structured as either one or two OFDM symbols. Each of those OFDM symbols contains a CP, which length is the same as the CP for data OFDM symbols. The time domain structure is exemplified in Figure 2.6. The frequency domain sequences for all full-bandwidth preambles are derived from the

sequence as shown in Figure 2.7. The frequency domain sequence for the 4 times 64 sequence $P_{4\times 64}$ is defined by Equation (2.3):

$$P_{4\times 64(k)} = \begin{cases} \sqrt{2}\cdot\sqrt{2}\cdot conj(P_{ALL}(k)) & k_{\bmod 4} = 0 \\ 0 & k_{\bmod 4} \neq 0 \end{cases} \tag{2.3}$$

The frequency domain sequence for the 2 times 128 sequence P_{even} is defined by Equation (2.4):

$$P_{even(k)} = \begin{cases} \sqrt{2}\cdot P_{ALL}(k) & k_{\bmod 2} = 0 \\ 0 & k_{\bmod 2} \neq 0 \end{cases} \tag{2.4}$$

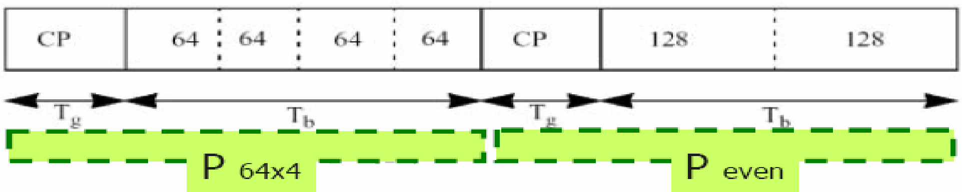

Figure 2.6: DL and network entry preamble structure

P_{ALL}(-100:100) = {1-j, 1-j, -1-j, 1+j, 1-j, 1-j, -1+j, 1-j, 1-j, 1-j, 1+j, -1-j, 1+j, 1+j, -1-j, 1+j, -1-j, -1-j, 1-j, -1+j, 1-j, 1-j, -1-j, 1+j, 1-j, 1-j, -1+j, 1-j, 1-j, 1-j, 1+j, -1-j, 1+j, 1+j, -1-j, 1+j, -1-j, -1-j, 1-j, -1+j, 1-j, 1-j, -1-j, 1+j, 1-j, 1-j, -1+j, 1-j, 1-j, 1-j, 1+j, -1-j, 1+j, 1+j, -1-j, 1+j, -1-j, -1-j, 1-j, -1+j, 1+j, 1+j, 1-j, -1+j, 1+j, 1+j, -1-j, 1+j, 1+j, 1+j, -1+j, 1-j, -1+j, -1+j, 1-j, -1+j, 1-j, 1-j, 1+j, -1-j, -1-j, -1-j, -1+j, 1-j, -1-j, -1-j, 1+j, -1-j, -1-j, -1-j, 1-j, -1+j, 1-j, 1-j, -1+j, 1-j, -1+j, -1+j, -1-j, 1+j, 0, -1-j, 1+j, -1+j, -1+j, -1-j, 1+j, 1+j, 1+j, -1-j, 1+j, 1-j, 1-j, 1-j, -1+j, -1+j, -1+j, -1+j, 1-j, -1-j, -1-j, -1+j, 1-j, 1+j, 1+j, -1+j, 1-j, 1-j, 1-j, -1+j, 1-j, -1-j, -1-j, -1-j, 1+j, 1+j, 1+j, 1+j, -1-j, -1+j, -1+j, 1+j, -1-j, 1-j, 1-j, 1+j, -1-j, -1-j, -1-j, 1+j, -1-j, -1+j, -1+j, -1+j, 1-j, 1-j, 1-j, 1-j, -1+j, 1+j, 1+j, -1-j, 1+j, -1+j, -1+j, -1-j, 1+j, 1+j, 1+j, -1-j, 1+j, 1-j, 1-j, 1-j, -1+j, -1+j, -1+j, -1+j, 1-j, -1-j, -1-j, 1-j, -1+j, -1-j, -1-j, 1-j, -1+j, -1+j, -1+j, 1-j, -1+j, 1+j, 1+j, 1+j, -1-j, -1-j, -1-j, -1-j, 1+j, 1-j, 1-j} (77)

Figure 2.7: Frequency domain sequences for all full-bandwidth preambles

For OFDMA mode, the first symbol of the DL transmission is the preamble and the preamble subcarriers are divided into three carrier-sets. Those subcarriers are modulated using a boosted BPSK modulation with a specific PN code. There are three possible groups consisting of a carrier-set each that may be used by any segment. Each segment uses a preamble composed of a carrier-set out of the three available carrier-sets in the following manner: (In the case of segment 0 under 2048-FFT, the DC carrier will

not be modulated at all and the appropriate PN will be discarded; therefore, DC carrier shall be always zero. For the preamble symbol, there will be 172 guard band subcarriers on the left side and the right side of the spectrum). For example, Figure 2.8 depicts the preamble of segment 1 for 2048-FFT.

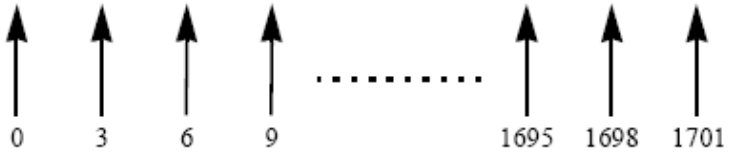

Figure 2.8: Example of DL preamble for segment 1

2.2 Key Features of Scalable OFDMA

Although IEEE 802.16-2005 is generally perceived as the mobile version of the standard, in reality it serves the dual purpose of adding extensions for mobility and including new enhancements to the OFDMA physical layer. This new enhanced IEEE 802.16-2005 physical layer is now being referred to as Scalable OFDMA (SOFDMA) and includes a number of important features for fixed, nomadic, and mobile networks. Because of these advantages, most of the industry will build their IEEE 802.16-2005 products using SOFDMA technology. However, the IEEE 802.16-2005 standard is not just for mobility. There are also many compelling reasons for using SOFDMA in fixed broadband wireless access (BWA) networks. In this section, we will focus on some key features of SOFDMA for fixed and mobile wireless applications [6], [7].

2.2.1 Scalable Channel Bandwidth

Scalability is one of the most important advantages of OFDMA. Spectrum resources for wireless broadband worldwide are still quite different in its allocation. With OFDMA subcarrier structure, it is designed to be able to scale to work in different

channelization from 1.25 to 20 MHz to cope with varied worldwide requirements as efforts proceed to achieve spectrum harmonization in the longer term. The scalability is supported by adjusting FFT size according to the different channel bandwidth to fix the subcarrier frequency spacing. By fixing the subcarrier spacing and symbol duration, the basic unit of physical resource is fixed. Therefore, the impact to higher layers is minimal when scaling the bandwidth.

The significant advantage from scalability is the flexibility of deployment. With the little modification to different air interfaces, OFDMA system can be deployed in various frequency bands to flexibly address the requirement for various spectrum allocation and usage model requirements. The OFDMA scalability parameters used in the thesis are listed in Table 2.4. The subcarrier spacing is fixed to 11.16 kHz and the symbol time is fixed to 89.6 us. With the flexibility to support wider range bandwidth, OFDMA also enjoys high sector throughput, which allows more efficient multiplexing of data traffic, lower latency and better QoS.

Table 2.4: OFDMA scalability parameters for different bandwidth

Parameters	Values				
Bandwidth (MHz)	1.25	2.5	5	10	20
Sampling frequency (MHz)	1.43	2.86	5.71	11.4	22.8
FFT size	128	256	512	1024	2048
Subcarrier spacing	11.16 KHz				
Useful symbol time (Tb)	89.6 us				
CP duration	22.4 us (Tb/4)				

2.2.2 Sub-channelization and Permutation

Active (data and pilot) subcarriers are grouped into subsets of subcarriers called subchannels. The OFDMA PHY supports sub-channelization in both DL and UL. The minimum frequency-time resource unit of sub-channelization is one slot, which is equal to 48 data tones. There are two major types of subcarriers permutation for subchannelization: *diversity* and *contiguous*. The diversity permutation takes subcarriers pseudo-randomly to form a subchannel. The diversity permutations include DL & UL PUSC (Partial Usage of Subchannels), DL FUSC (Full Usage of Subchannels), and additional optional permutations. The contiguous permutation groups a block of adjacent sub-carriers to form a subchannel. The contiguous permutations include DL & UL AMC (Adaptive Modulation and Coding). With DL PUSC, for each pair of OFDM symbols, the usable subcarriers are grouped into *clusters* containing 14 adjacent subcarriers per symbol, with pilot and data allocations in each cluster in the even and odd symbols as shown in Figure 2.9.

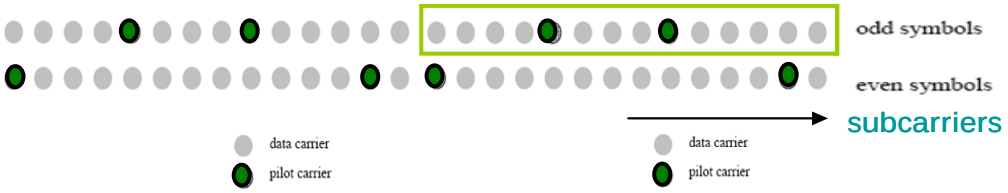

Figure 2.9: Cluster structure for PUSC

Divide these clusters into several *Major Grou*ps. The allocation algorithm varies with FFT sizes. For each subchannel, subcarriers are distributed in some clusters that belong to its major group as shown in Figure 2.10. A subchannel contains 2 clusters and is comprised of 48 data subcarriers and 8 pilot subcarriers. Allocating subcarriers to subchannel in each major group is performed separately for each OFDMA symbol by first allocating the pilot carriers within each cluster, and then taking all remaining data

carriers within the symbol and using the procedure described in Equation (2.5):

$$subcarrier(k,s) = N_{subchannels} \cdot n_k + \{p_s[n_k \bmod N_{subchannels}] + DL\_PermBase\} \bmod N_{subchannels} \quad (2.5)$$

where

$subcarrier(k,s)$ is the subcarrier index k in subchannel s

$N_{subchannels}$ is the number of subchannels in current partitioned major group

$n_k = (k + 13 \cdot s) \bmod N_{subccarriers}$

$N_{subccarriers}$ is the number of data subcarriers allocated to a subchannel

$p_s[j]$ is the series obtained by rotating basic permutation sequence cyclically to the left s times

The parameters vary with FFT sizes. Figure 2.11 shows an example of mapping OFDMA slots into subchannels and symbols in the DL PUSC.

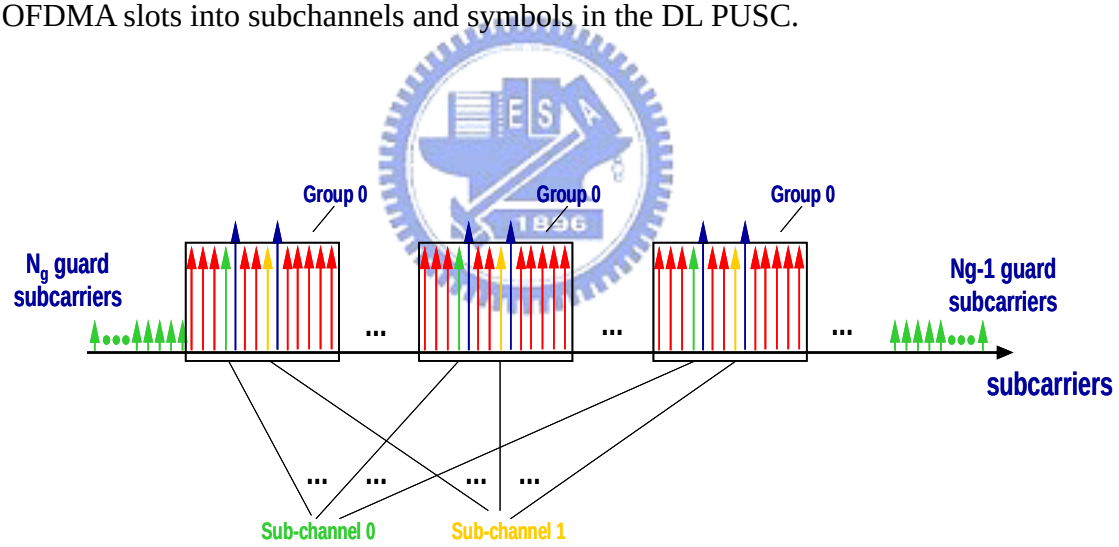

Figure 2.10: Allocated subcarriers into subchannels for PUSC

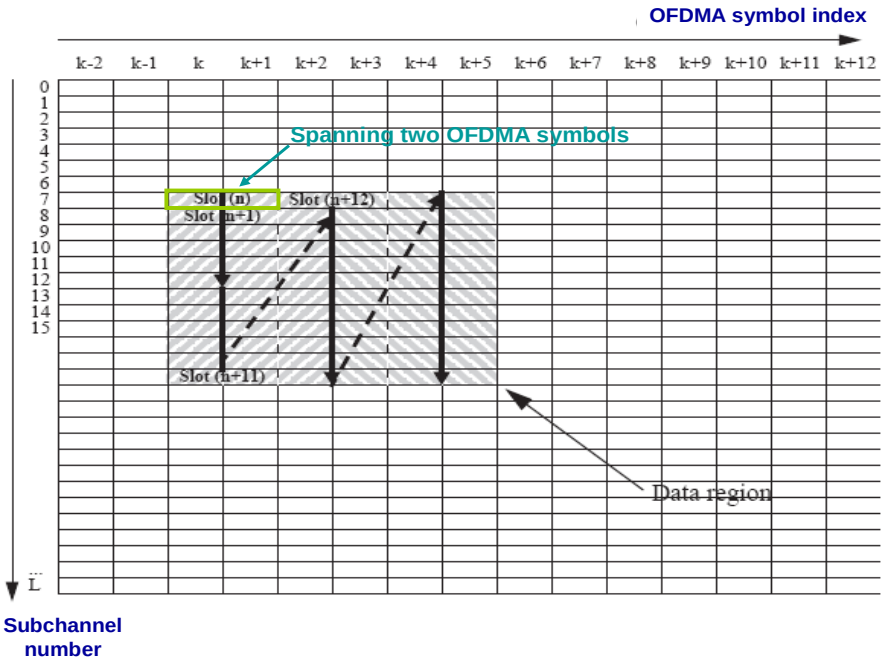

Figure 2.11: Example of mapping OFDMA slots to subchannels and symbols in DL PUSC

Compared with the cluster structure for DL PUSC, a *tile* structure is defined for the UL PUSC whose format is shown in Figure 2.12. The slot is comprised of 48 data subcarriers and 24 pilot subcarriers in 3 OFDM symbols.

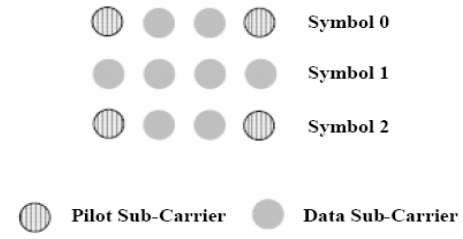

Figure 2.12: Description of a UL PUSC tile

FUSC achieves full diversity by spreading tones over entire band. The symbol structure is constructed using pilots, data, and zero subcarriers. The symbol is first allocated with the appropriate pilots and with zero subcarriers, and then all the remaining subcarriers are used as data subcarriers. To allocate the data subchannels, the remaining subcarriers are partitioned into groups of contiguous subcarriers. Each

subchannel consists of one subcarrier from each of these groups as shown in Figure 2.13. The number of groups is therefore equal to the number of subcarriers per subchannel. The exact partitioning into subchannels is according to the same procedure as Equation (2.5).

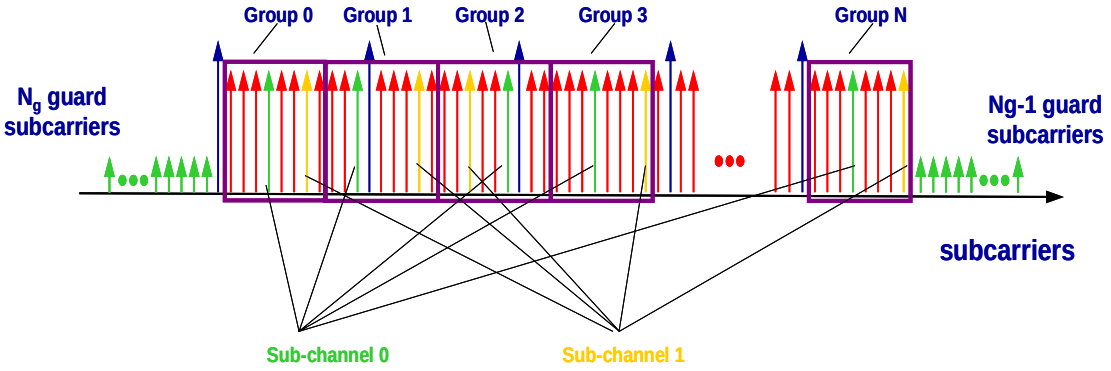

Figure 2.13: Allocated subcarriers into subchannels for FUSC

The contiguous permutation groups a block of adjacent subcarriers to form a subchannel, such as DL AMC and UL AMC. As shown in Figure 2.14, a bin consists of 9 adjacent subcarriers in a symbol, with 8 tones for data and one assigned for a pilot. A *slot* in AMC is defined as a collection of bins of the type (N x M = 6), where N is the number of adjacent bins and M is the number of adjacent symbols. Thus 4 different ways of defining a slot are (6 bins, 1 symbol), (3 bins, 2 symbols), (2 bins, 3 symbols), (1 bin, 6 symbols). AMC permutation enables multi-user diversity by choosing the sub-channel with the best channel frequency response.

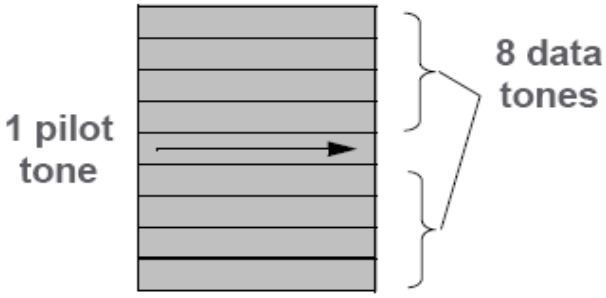

Figure 2.14: AMC bin structure

In general, diversity subcarrier permutations perform well in mobile applications while contiguous subcarrier permutations are well suited for fixed, portable, or low mobility environments. These options enable the system designer to trade-off mobility for throughput.

2.2.3 Fractional Frequency Reuse

In OFDMA mode, users operate on subchannels which only occupy a small fraction of the channel bandwidth and the cell edge interference problem can be easily solved by reconfiguration of the subchannel usage without resorting to traditional frequency planning. In mobile applications, the flexible subchannel reuse is facilitated by subchannel segmentation and permutation zone. A segment is a subdivision of the available OFDMA subchannels (one segment may include all subchannels). Permutation Zone is a number of contiguous OFDMA symbols in DL or UL that use the same permutation. The DL or UL subframe may contain more than one permutation zone.

The subchannel reuse pattern can be configured so that users close to the base station operate on the zone with all subchannels available. While for the edge users, each cell and sector operates on the zone with a fraction of all subchannels available. In Figure 2.15, F1, F2 and F3 are different sets of subchannels in the same frequency channel. With this configuration, the full load frequency reuse of one is maintained for center users to maximize spectral efficiency while fractional frequency reuse is achieved for edge users to improve edge user connection quality and throughput. The subchannel reuse planning can be dynamically optimized across sectors or cells based on network load and interference conditions on a frame by frame basis. All the cells and sectors therefore, can operate on the same frequency channel without the

requirement for frequency planning.

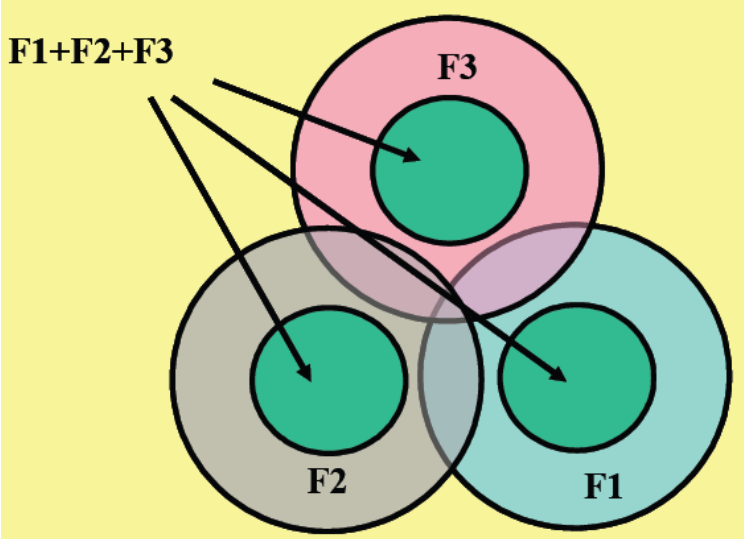

Figure 2.15: Description of fractional frequency reuse

2.3 Transmit Techniques

In order to increase the range and reliability of WiMAX systems, the WiMAX standard supports optional multiple-antenna techniques such as Alamouti Space-Time Coding (STC), Adaptive Antenna Systems (AAS) and Multiple-Input Multiple-Output (MIMO) systems.

There are several advantages to using multiple-antenna technology over single-antenna technology:

• Array Gain: This is the gain achieved by using multiple antennas so that the signal adds coherently.

• Diversity Gain: This is the gain achieved by utilizing multiple paths so that the probability that any one path is bad does not limit performance. Effectively, diversity gain refers to techniques at the transmitter or receiver to achieve multiple “looks” at the fading channel. These schemes improve performance by increasing the stability of the

received signal strength in the presence of wireless signal fading. Diversity may be exploited in the spatial (antenna), temporal (time), or spectral (frequency) dimensions.

• Co-channel Interference Rejection (CCIR): This is the rejection of signals by making use of the different channel response of the interferers.

2.3.1 Transmit Diversity: Space-Time Coding

In order to increase the rate and range of the modem, there are several considerations. Generally, BS can bear more cost and complexity than SS, so multiple-antenna techniques are a good option at BS, also called transmit diversity. Among various transmit diversity schemes, STC is the most popular scheme with the feature of open loop (i.e., no feedback signaling is required) as channel information is not required at the transmitter. Therefore we will focus on the scheme of STC with 2 transmit antennas in this section as shown in Figure 2.16.

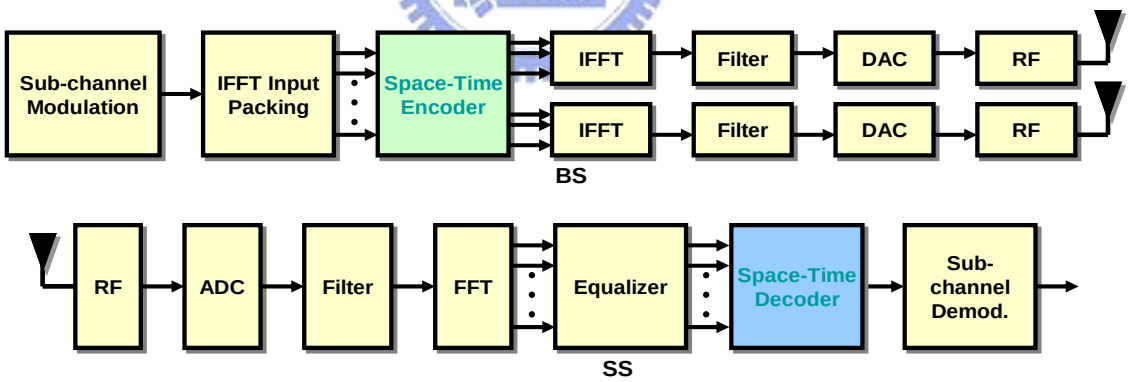

Figure 2.16: Block diagram of STC

The space-time block coding scheme was first discovered by Alamouti for two transmit antennas. Symbols transmitted from those antennas are encoded in both space and time in a simple manner to ensure that transmissions from both the antennas are orthogonal to each other. This would allow the receiver to decode the transmitted

information with a slight increment in the computational complexity.

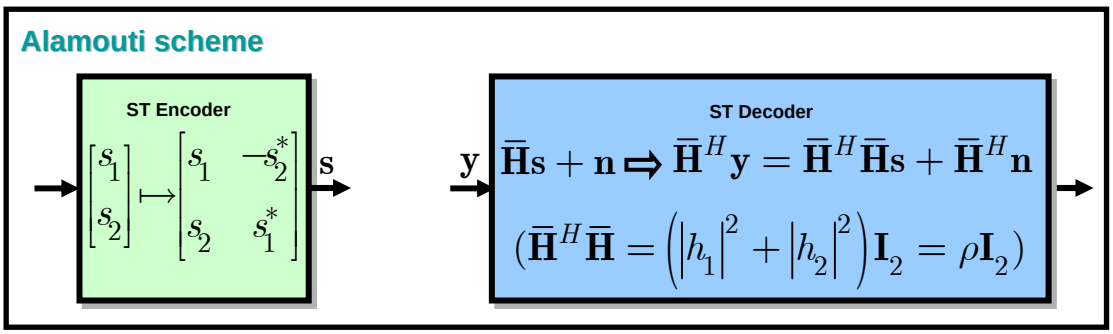

Figure 2.17: Illustration of Alamouti scheme

Figure 2.17 shows the operation of Alamouti scheme. The input symbols to the space-time block encoder are divided into groups of two symbols. At a given symbol period, the encoder takes a block of two modulated symbols s_1 and s_2 in each encoding operation and maps them to the transmit antennas according to a code matrix given by

$$\mathbf{s} = \begin{bmatrix} s_1 & -s_2^* \\ s_2 & s_1^* \end{bmatrix} \tag{2.6}$$

The encoder outputs are transmitted in two consecutive transmission periods from two transmit antennas. Let h_1 and h_2 be the channel gains from the first and second transmit antennas to the only one receiver antenna. Assume that h_1 and h_2 are scalar and constant over two consecutive symbol periods. The received signals in two consecutive symbol periods, denoted as r_1 and r_2, can be expressed as

$$\begin{aligned} r_1 &= h_1 s_1 + h_2 s_2 + n_1 \\ r_2 &= -h_1 s_2^* + h_2 s_1^* + n_2 \end{aligned} \tag{2.7}$$

where n_1 and n_2 are AWGN noise modeled as identical independent distributed (i.i.d.)

complex Gaussian random variables with zero mean and power spectral density $N_0/2$ for each dimension. The above equation can be rewritten in a matrix form as

$$\mathbf{r} = \begin{bmatrix} r_1 \\ r_2^* \end{bmatrix} = \underbrace{\begin{bmatrix} h_1 & h_2 \\ (h_2)^* & -(h_1)^* \end{bmatrix}}_{\overline{\mathbf{H}}} \underbrace{\begin{bmatrix} s_1 \\ s_2 \end{bmatrix}}_{\mathbf{s}} + \underbrace{\begin{bmatrix} n_1 \\ n_2^* \end{bmatrix}}_{\mathbf{n}} = \overline{\mathbf{H}} \cdot \mathbf{s} + \mathbf{n} \tag{2.8}$$

Since the channel matrix $\overline{\mathbf{H}}$ is unitary, i.e. $\overline{\mathbf{H}}^H \overline{\mathbf{H}} = \rho \cdot \mathbf{I_2}$, where $\rho = |h_1|^2 + |h_2|^2$, the ML decoder can perform an MRC operation on the modified signal vector $\tilde{\mathbf{r}}$ given by

$$\begin{aligned} \tilde{\mathbf{r}} &= \overline{\mathbf{H}}^H \cdot \mathbf{r} = \rho \cdot \mathbf{s} + \underbrace{\overline{\mathbf{H}}^H \cdot \mathbf{n}}_{\tilde{\mathbf{n}}} \\ &= \rho \cdot \mathbf{s} + \tilde{\mathbf{n}} \end{aligned} \tag{2.9}$$

Therefore, we can obtain the space-time decoded vector $\mathbf{s}$.

In OFDM-256 mode, the preamble for Alamouti transmission is transmitted from both antennas with the even subcarriers used for antenna 1 and the odd subcarriers used for antenna 2. This means that each set of data requires to be appropriately smoothed. The pilots have certain degenerate situations: for the first Alamouti transmitted symbol, the pilots destructively add and for the second Alamouti transmitted symbol, the pilots constructively add. Hence, the pilots cannot always be useful. Properly processing the pilot symbols is required.

For OFDMA mode, STC coding is done on all data subcarriers that belong to an STC coded burst in the two consecutive OFDMA symbols. Pilot subcarriers are not encoded and are transmitted from either antenna 0 or antenna 1. In PUSC, the pilot allocation to cluster is changed as shown in Figure 2.18. The pilot locations change in period of 4 symbols to accommodate two antennas transmission with the same estimation capability.

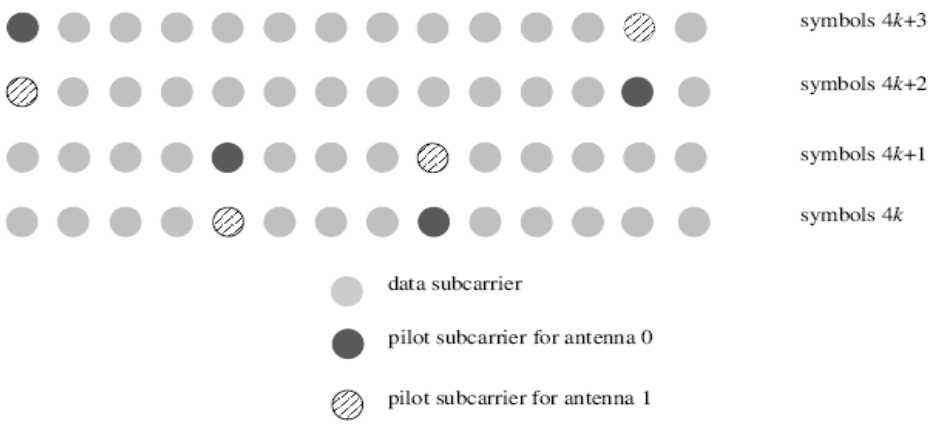

Figure 2.18: Cluster structure for STC PUSC using two antennas

2.3.2 Transmit Beamforming: Adaptive Antenna System

Future wireless communication systems are aimed to provide higher data rates with better link quality subject to being *interference limited*. Smart antenna technology is one of the most promising technologies for increasing both system coverage and capacity as shown in Figure 2.19. AAS, although an optional feature, through the use of more than one antenna elements at BS, can significantly improve range and capacity by adapting the antenna pattern and concentrating its radiation to each individual user. There are several advantages of using beamforming:

- Increase spectral efficiency proportional to the number of antenna elements
- Realize an inter-cell frequency reuse of one and an in-cell reuse factor proportional to the number of antenna elements
- Reduce interference by steering nulls in directions of co-channel interferers
- Increase SNR of certain subscribers and steer nulls to others that can enable bursts to be concurrently transmitted to spatially separated users.

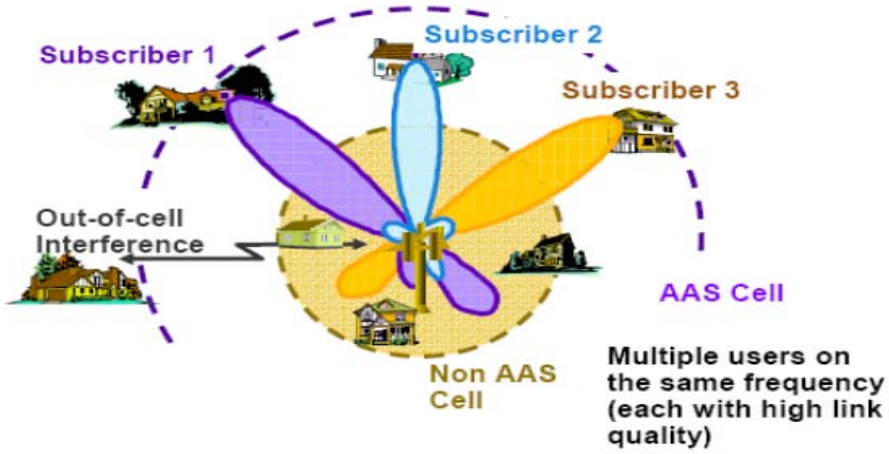

Figure 2.19: Illustration of AAS

First, the generalized AAS zone allocation is introduced as shown in Figure 2.20. The frame is divided into two parts: the fist part is allocated to the non-AAS users and the second part (called AAS zone) is allocated to the AAS users. This allows a mixture of non-AAS and AAS users to be supported by the same BS. The BS can dynamically allocate capacity to non-AAS and AAS traffic. The SS without AAS capability will ignore the traffic in the AAS zone. In the following paragraphs, we will introduce the AAS operations for OFDM mode and OFDMA mode individually.

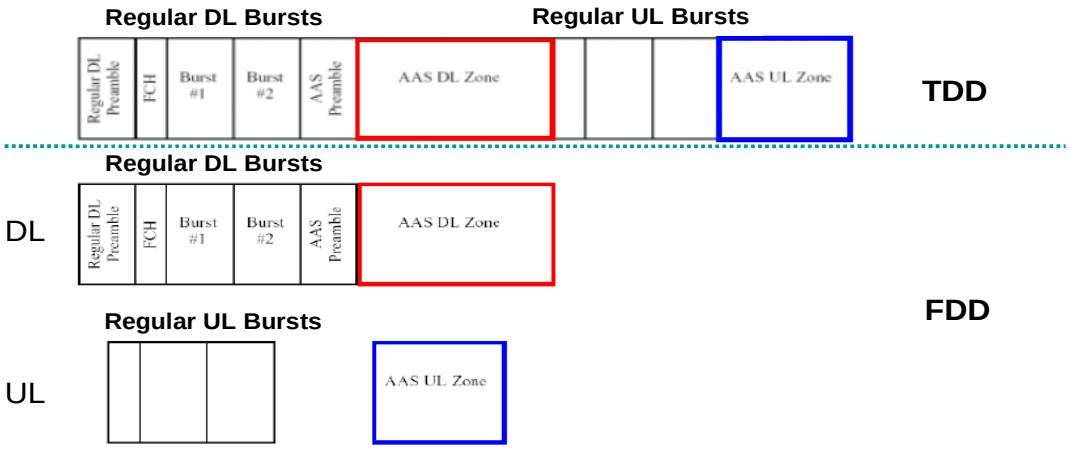

Figure 2.20: Generalized AAS zone allocation

OFDM

Figure 2.21 shows the AAS zone structure in OFDM mode. AAS preamble consists of two OFDM symbols, which can be transmitted from up to four beams. For a SS to distinguish one beam from another, the 200 subcarriers are divided into four groups, with each group transmitted on one beam. Supposing that the 200 subcarriers are represented by their frequency offset index, *k*, relative to the central carrier, ie, *k*=-100,-99,…,-2,-1,1,2,…,99,100, the AAS preamble transmitted on beam *m*, *m*=0,1,2,3, is defined as those subcarriers with k mod 4. The AAS preamble is used by AAS SS to perform channel estimation on each beam. Each DL burst starts with one or several repetitions of a preamble plus FCH pair. The FCH contains the information about location and transmission parameters for the data burst. This pair may be transmitted on a directed beam, or optionally transmitted on several beams to improve the reliability of the FCH reception. Operation of AAS requires feedback of channel state information. For OFDM mode, AAS-FBCK-REQ is used for assisting beamforming and SS performs the measurement from AAS preamble that belongs to its burst. AAS-BEAM-REQ is used for beam adjustment and SS performs the measurement on specified beams requested by BS.

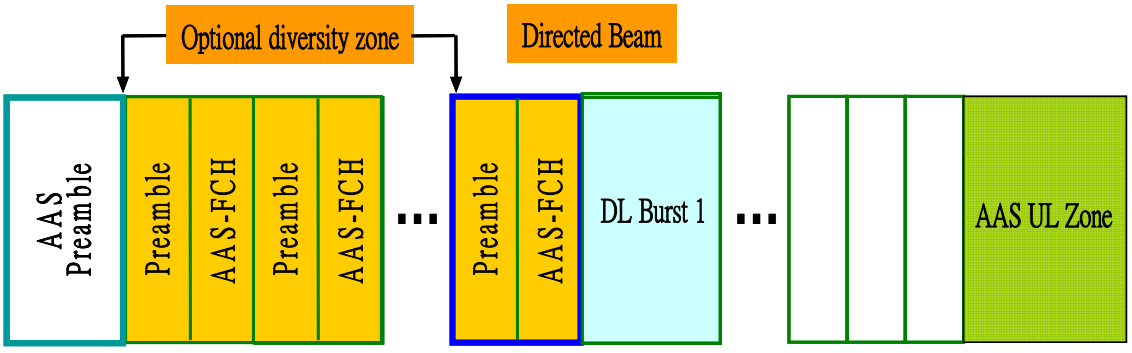

Figure 2.21: AAS zone structure in OFDM mode

OFDMA

Figure 2.22 shows the AAS zone structure in OFDMA mode. AAS_DLFP in an AAS zone is preceded by an AAS DL preamble of one symbol duration. All other data bursts within an AAS zone have a preamble whose duration is specified in AAS_DL_IE. AAS_DLFP provides a robust transmission of required BS parameters to enable SS access allocation. Each AAS_DLFP requires not carry the same information. Different beams may be used within the AAS diversity map zone. For OFDMA mode, REP-RSP MAC message shall be sent by SS in response to a REP-REQ message from the BS to report estimation of the mean DL CINR (carrier-to-interference-and-noise ratio).

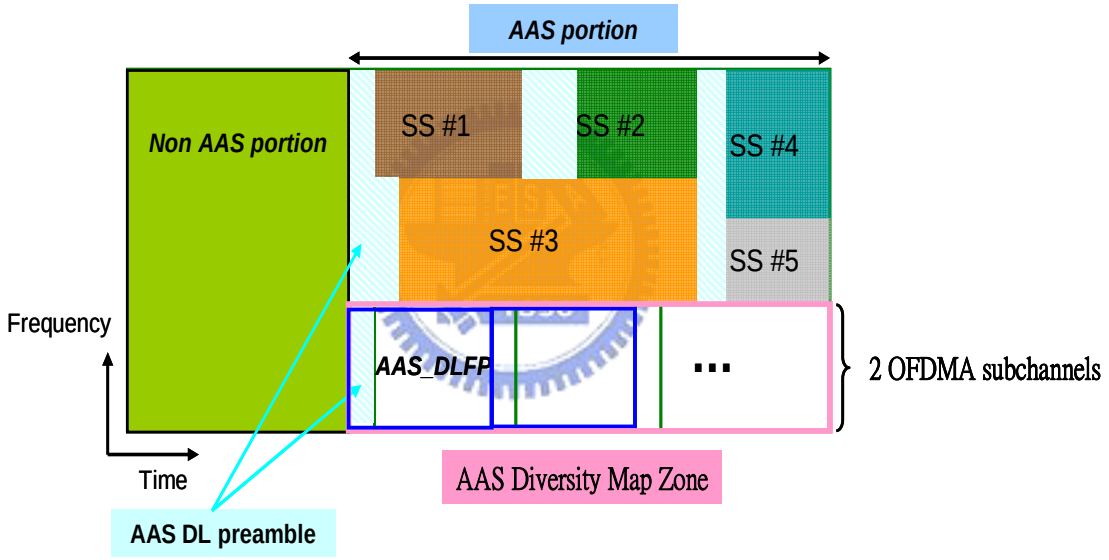

Figure 2.22: AAS zone structure in OFDMA mode

2.4 Summery

Specification of IEEE 802.16 system has been introduced in this chapter. Unlike the CDMA-based 3G systems, which have evolved from voice-centric systems, WiMAX is designed to meet the requirements necessary for the delivery of broadband data services as well as voice. The Mobile WiMAX physical layer is based on Scalable OFDMA technology. The new technologies employed for Mobile WiMAX result in lower equipment complexity and simpler mobility management due to the all-IP core

network and provide Mobile WiMAX systems with many advantages over CDMA based 3G systems. We also introduce some key transmit techniques and their operations. By using these transmit techniques, the capacity and range of the system can be improved significantly.

Chapter 3

Channel Estimation and Synchronization for WiMAX System

In this chapter, channel estimation and synchronization schemes are introduced. In real situations, synchronization and channel estimation should be done before data detection. First, two channel models corresponding to static or mobile environments are introduced in Section 3.1. Second, a jointly designed timing and frequency synchronization scheme is proposed in Section 3.2 and then computer simulations will be showed to confirm the performance of the proposed scheme. In Section 3.3, two channel estimation schemes are introduced to deal with different environments. Finally, Section 3.4 will describe the phase estimation and the residual frequency offset estimation scheme, and then computer simulations show that more accurate frequency synchronization can be obtained after compensating the residual frequency offset.

3.1 Channel Model

Wireless propagation channels have been studied for more than 50 years, and a large number of channel models are already available. The signal that has propagated through a wireless channel consists of multiple echoes of the originally transmitted signals; this phenomenon is known as multipath propagation. The different multipath components are characterized by different attenuations and delays. The correct modeling of the parameters describing the multipath components is the key point of channel modeling.

In first generation systems, a super-cell architecture is used where the base station and subscriber station are in LOS condition and the system uses a single cell with no co-channel interference. For second generation systems, a scalable multi-cell architecture with NLOS conditions becomes necessary. In WiMAX system, the wireless channel is characterized by:

- Path loss (including shadowing)
- Multipath delay spread
- Fading characteristics
- Doppler spread

The main channel models were considered here: Stanford University Interim (SUI) channel models [11] and International Telecommunication Union (ITU) channel models [12]. Each channel model was parameterized in order to best fit the particular channel characteristics. SUI channel models can be used for simulations, design, and testing of technologies suitable for fixed broadband wireless applications. However, ITU channel models are applied for the measurement based channel model. Even though multipath parameters are fixed in a measurement based channel model, it is useful to reflect the real operating channel conditions.

3.1.1 SUI Channel Model for Fixed Wireless Application

SUI channel models were proposed in [11] to model a statistic environment in IEEE 802.16d. There are many possible combinations of parameters to obtain different channel descriptions. A set of 6 typical channels were selected for the three terrain types that are typical of the continental US. The channel parameters are related to terrain type, delay spread, and antenna directionality and each channel model has three taps with distinct K-factor and average power. Table 1 shows an example of time domain attribute of the SUI-3 channel, which is chosen to evaluate the proposed algorithm.

Table 3.1: Parameters of SUI-3 channel models

SUI – 3 Channel				
	Tap 1	**Tap 2**	**Tap 3**	**Units**
Delay	0	0.4	0.9	μs
Power (omni ant.)	0	-5	-10	dB
90% K-fact. (omni)	1	0	0	
75% K-fact. (omni)	7	0	0	
Doppler	0.4	0.3	0.5	Hz
Antenna Correlation:	$\rho_{ENV} = 0.4$			
Gain Reduction Factor:	GRF = 3 dB			
Normalization Factor:	$F_{omni} = -1.5113$ dB, $F_{30°} = -0.3573$ dB			

Multipath Delay Profile

Due to the scattering environment, the channel has a multipath delay profile. It is characterized by τ_{rms} (RMS delay spread of the entire delay profile) which is defined as

$$\tau_{rms}^2 = \sum_j P_j \tau_j^2 - (\tau_{avg})^2 \tag{3.1}$$

where

$\tau_{avg} = \sum_j P_j \tau_j$,

τ_j is the delay of the *j*th delay component of the profile and P_j is given by

P_j = (power in the *j*th delay component) / (total power in all components)

RMS delay spread

A delay spread model was based on a large body of published reports. It was found that the RMS delay spread follows lognormal distribution and that the median of this distribution grows as some power of distance. The model was developed for rural, suburban, urban, and mountainous environments. The model is of the following form

$$\tau_{rms} = T_1 d^{\varepsilon} y \tag{3.2}$$

where τ_{rms} is the RMS delay spread, d is the distance in km, T_1 is the median value of τ_{rms} at d = 1 km, ε is an exponent that lies between 0.5-1.0, and y is a lognormal variant. Depending on the terrain, distance, antenna directivity and other factors, the RMS delay spread values can span from very small values (tens of nanoseconds) to large values (microseconds).

Fading distribution, K-factor

The narrow band received signal fading can be characterized by a Ricean fading. The key parameter of this distribution is the K-factor, defined as the ratio of the “fixed” component power and the “scatter” component power. The narrow band K-factor distribution was found to be lognormal, with the median as a simple function of season, antenna height, antenna beamwidth and distance. The model for the K-factor (in linear scale) is as follows:

$$K = F_s F_h F_b K_o d^{\gamma} u \tag{3.3}$$

where

F_s is a season factor; F_s =1.0 in summer; 2.5 in winter

F_h is the received antenna height factor

F_b is the beamwidth factor

K_o and γ are regression coefficients

u is a lognormal variable which has 0 dB mean and a standard deviation of 8 dB.

Using this model, one can observe that the K-factor decreases as the distance increases and as antenna beamwidth increases.

Doppler spectrum

The random components of the coefficients generated in the previous paragraph have a white spectrum since they are independent of each other. The SUI channel model defines a specific power spectral density (PSD) function for these scatter component channel coefficients called "rounded" PSD which is given as

$$S(f) = \begin{cases} 1 - 1.72 f_0^2 + 0.785 f_0^4 & |f_0| \le 1 \\ 0 & |f_0| > 1 \end{cases} \tag{3.4}$$

where $f_0 = \frac{f}{f_m}$. In fixed wireless channels the shape of the spectrum is therefore different than the classical Jake's spectrum for mobile channels. Figure 3.1 shows that its shape of Doppler spectrum is convex.

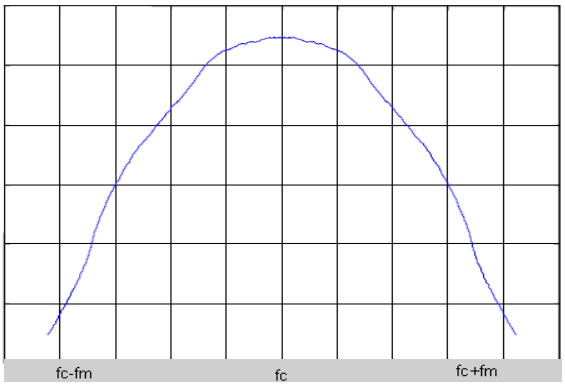

Figure 3.1: Doppler spectrum of SUI channel models

Antenna correlation

The SUI channel models define an antenna correlation, which has to be considered if multiple transmit or receive elements, i.e. multiple channels, are being simulated. Antenna correlation is commonly defined as the envelope correlation coefficient between signals transmitted at two antenna elements. The received baseband signals are modeled as two complex random processes *X(t)* and *Y(t)* with an envelope correlation coefficient of

$$\rho_{env} = \left| \frac{E\left\{ \left(X - E\{X\} \right) \left(Y - E\{Y\} \right)^* \right\}}{\sqrt{E\left\{ \left| X - E\{X\} \right|^2 \right\} E\left\{ \left| Y - E\{Y\} \right|^2 \right\}}} \right| \tag{3.5}$$

Note that this is not equal to the correlation of the envelopes of two signals, a measure that is also used frequently in cases where no complex data is available.

Antenna gain reduction factor

The use of directional antennas requires to be considered carefully. The gain due to the directivity can be reduced because of the scattering. The effective gain is less than the actual gain. This factor should be considered in the link budget of a specific receiver antenna configuration.

Denote ΔG_{BW} as the Gain Reduction Factor. This parameter is a random quantity which dB value is Gaussian distributed with a mean μ_{grf} and a standard deviation σ_{grf} given by

$$\mu_{grf} = -(0.53 + 0.1\mathrm{I}) \ln(\beta / 360) + (0.5 + 0.04\mathrm{I})(\ln(\beta / 360))^2 \tag{3.6}$$

$$\sigma_{grf} = -(0.93 + 0.02\mathrm{I}) \ln(\beta / 360) \tag{3.7}$$

where

β is the beamwidth in degrees

I = 1 for winter and I = -1 for summer

In the link budget computation, if G is the gain of the antenna (dB), the effective gain of the antenna equals $G - \Delta G_{BW}$. For example, if a 20-degree antenna is used, the mean value of ΔG_{BW} would be closed to 7 dB.

3.1.2 ITU Channel Model for Mobile Wireless Application

As we know, for fixed wireless application such as IEEE 802.16-2004, the SUI channel models are recommended for simulation. However, for mobile wireless application like IEEE 802.16-2005, the recommendatory channel model is not proposed at present. Here we choose International Telecommunication Union (ITU) channel model [12] for mobile and fixed use.

ITU channel model is a measurement based channel model proposed for the 3GPP WCDMA system. Delay and average power of each multipath for the ITU channel models are summarized in Table 3.2. Four or six multipath signals are generated in the wireless channel depending on the channel type as shown in Table 3.2 respectively. The ITU channel model can be modeled as

$$w(t) = \sum_{n=1}^{N} \sqrt{p_n}\, g_n(t) z(t - \tau_n) \tag{3.8}$$

where *z(t)* and *w(t)* denote the complex low pass representations of the channel input and output respectively, p_n is the strength of the *n*th weight and $g_n(t)$ is the complex Gaussian process weighting the *n*th replica.

Table 3.2: Parameters of ITU channel models

Channel Profile \ Multipath		M1	M2	M3	M4	M5	M6
Pedestrian A	Delay (ns)	0	110	190	410	NA	NA
($M = 4$)	Power (dB)	0	-9.7	-19.2	-22.8		
Pedestrian B	Delay (ns)	0	200	800	1200	2300	3700
($M = 6$)	Power (dB)	0	-0.9	-4.9	-8.0	-7.8	-23.9
Vehicular A	Delay (ns)	0	310	710	1090	1730	2510
($M = 6$)	Power (dB)	0	-1.0	-9.0	-10.0	-15.0	-20.0
Vehicular B	Delay (ns)	0	300	8900	12900	17100	20000
($M = 6$)	Power (dB)	-2.5	0	-12.8	-10.0	-25.2	-16.0

As shown in Table 3.2, ITU channel model includes two environments. For the pedestrian test environment, this environment is characterized by small cells and low transmit power. Base stations with low antenna height are located outdoors, and pedestrian users are located on streets, inside buildings or residences. Its path loss is defined by

$$L = 40\log_{10}R + 30\log_{10}f + 49 \quad \text{(dB)} \tag{3.9}$$

where R denotes the separation (km) between the base station and the mobile station and f is carrier frequency.

For vehicular environment, it is characterized by large cells and higher transmit power. The model is applicable for in urban and suburban areas outside the high rise core where the buildings are of nearly uniform height. Its path loss is written as

$$L = 40(1 - 4\times10^{-3}\,\Delta h_b)\log_{10}R - 18\log_{10}\Delta h_b + 21\log_{10}f + 80 \quad \text{(dB)} \tag{3.10}$$

where

R is the separation (km) between base station and mobile station

f is carrier frequency

Δh_b is base station antenna height (m), measured from the average rooftop level

The path loss model is valid for a range of Δh_b from 0 to 50 m.

The ITU channel model uses Doppler spectrum of classical Jake's spectrum. As shown in Figure 3.2, the Doppler spectrum is concave.

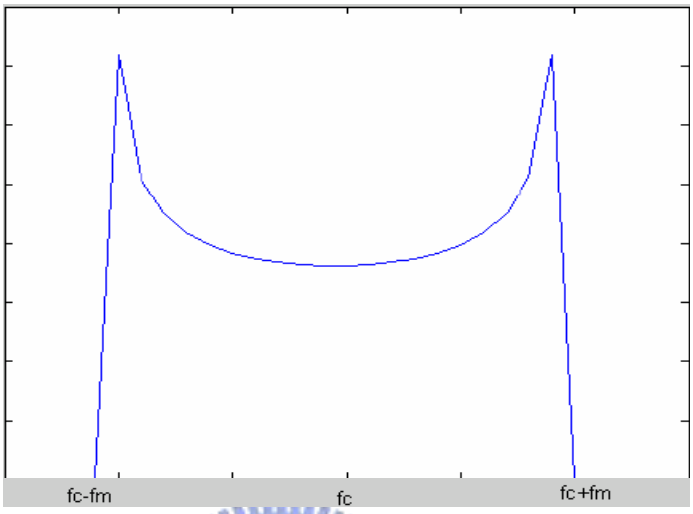

Figure 3.2: Doppler spectrum of ITU channel models

3.2 Timing and Frequency Synchronization

A joint design of timing and frequency synchronization scheme is proposed in this section [13], [14]. Synchronization should be done before the rest work like channel estimation and data detection. Here, we consider three steps to complete the timing and frequency synchronization:

(i) adjust the window size according to the known preamble structure and compute the delay correlation outputs;

(ii) use the delay correlation outputs to perform the timing synchronization;

(iii) use the corresponding delay correlation outputs to perform the frequency synchronization.

Before performing the timing and frequency synchronization algorithms, the received signal is passed through a matched filter. The delay correlation outputs can be obtained by correlating the received signal and the known preamble over a window of v

samples. The window size depends on the preamble structure. Here, CP length is configured to be 1/4 of FFT length for simplicity. The delay correlation outputs ψ_L and ψ_R of the *i*th received samples can be written as

$$\psi_{L,n}(i) = \sum_{k=0}^{v-1} \left(s_L^* \cdot r_{i+(n-1)\cdot f+k} \right)$$

$$\psi_{R,n}(i) = \sum_{k=0}^{v-1} \left(s_R^* \cdot r_{i+(n-1)\cdot f+k+v} \right), \quad (3.11)$$

where s_L and s_R denote the {1,*v*} and {*v*+1,2×*v*} samples of the known short preamble respectively, *v* is equal to half of short preamble length, *f* equals short preamble length, and *n* equals 1, 2, 3, and 4. There are 8 delay correlation outputs will be stored in each received samples.

In the following paragraphs, timing and frequency synchronization schemes which make use of the delay correlation outputs to achieve synchronization will be introduced.

- Timing synchronization: Timing synchronization involves finding the most significant path and the best possible time instant of the start of received data. After collecting groups of 8 delay correlation outputs obtained in Equation (3.11), the best timing instant can be detected by choosing the peak value of $\Psi(i)$ which is computed by

  $$\Psi(i) = \sum_{n=1}^{z/2} \left| \psi_{R,n}(i) \right|^2 + \sum_{n=1}^{z/2} \left| \psi_{L,n}(i) \right|^2, \quad (3.12)$$

  where $\Psi(i)$ represents the timing acquisition metric, and *z* is the number of delay correlation outputs for the *i*th received samples and equals 8. Once the best starting position of the received signal is detected, frequency synchronization can then be performed.

- Frequency synchronization: Frequency synchronization deals with finding a wider range of the frequency offset between the transmitter and receiver local oscillators. The frequency offset estimation is developed by choosing the delay correlation

outputs that make a peak value of $\Psi(i)$. Hence a frequency offset estimate can be found based on the phase of the delay correlation outputs as follows:

$$\Delta f = \frac{1}{2\pi T}\angle\left\{\phi_{d_{opt}}\right\} \tag{3.13}$$
$$= \frac{1}{2\pi T}\angle\left\{\sum_{n=1}^{z/2-1}\psi_{L,n}(i)\psi^{*}_{L,n+1}(i)+\sum_{n=1}^{z/2-1}\psi_{R,n}(i)\psi^{*}_{R,n+1}(i)\right\}$$

where T is the duration of the short preamble, d_{opt} is the optimum timing acquisition instant, and z is the number of delay correlation outputs for the ith received samples. Although the residual frequency offset still exists, it can be estimated by using the pilot subcarriers embedded in the data symbols that will be introduced in Section 3.4.

Computer simulations for the joint design of timing and frequency synchronization scheme are shown in Figures 3.3 and 3.4. First, Figure 3.3 shows the matched filter output of the proposed timing synchronization algorithm in a SISO-OFDM system. The simulation is carried out in the environment of ITU Vehicular B channel and simulated at $E_b/N_0 = 0$ dB. As seen in Figure 3.3, the jointly designed algorithm with timing synchronization gives satisfactory result in the mobile and Rayleigh fading channel. The start of the received signal can be estimated directly by detecting the peak of the timing acquisition metric $\Psi(i)$.

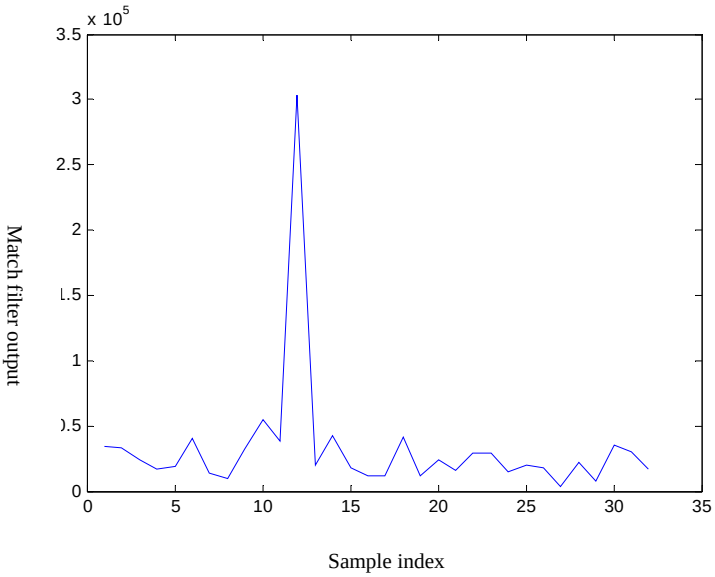

Figure 3.3: Matched filter output of the jointly designed algorithm for timing synchronization under ITU Vehicular B channel model (at $E_b/N_0 = 0$ dB)

Figure 3.4 shows the MSE of the frequency offset estimate as a function of E_b/N_0 in a SISO-OFDM system. SUI-3 channel model is used in this simulation. With the frequency offset estimation method, the average MSE is about 3×10^{-3}. For the scenario in which the oscillator offset is 20 kHz (about 10 ppm of the carrier frequency), the error of the frequency offset estimation method is just 60 Hz, which is much smaller than the subcarrier spacing.

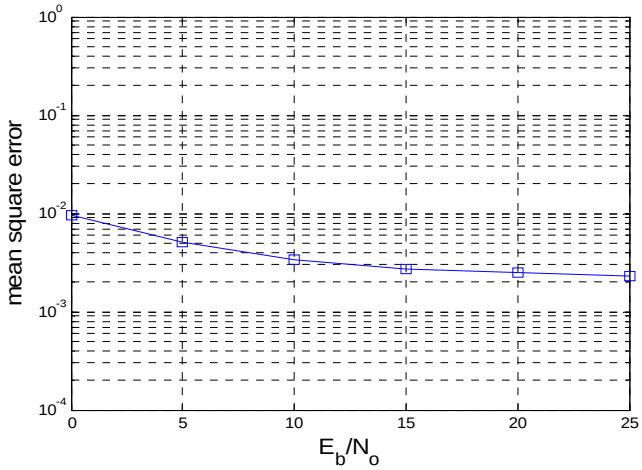

Figure 3.4: MSE of the jointly designed algorithm for frequency synchronization under SUI-3 channel model

3.3 Channel Estimation

This section describes two channel estimation schemes to deal with different environments. After finding the packet starting point, channel estimation is performed to recover the channel frequency response. Preamble-aided channel estimation is suitable for static environment. However, pilot-aided channel estimation provides better performance than preamble-aided channel estimation in mobile environment. In the following we introduce the operations of two schemes [15], [16].

- Preamble-aided channel estimation: Preamble-aided channel estimation is carried out by using the long preamble. Owing to the same symbol structure as data symbols, long preamble becomes the best candidate for performing this job. After removing CP, a receiver can perform channel estimation by taking FFT of the received long preamble to obtain the LS channel estimate

$$H_{LP} = \frac{R_{LP}}{FFT\{l_{LP}\}} \tag{3.14}$$

where R_{LP} is the received long preamble after taking FFT and l_{LP} is the known long preamble. As shown in Figure 3.5, after taking FFT of received long preamble, we also require to transform the original long preamble into frequency domain. Thus, the channel frequency response can be obtained simply by dividing the FFT output of received long preamble and the FFT output of the original long preamble.

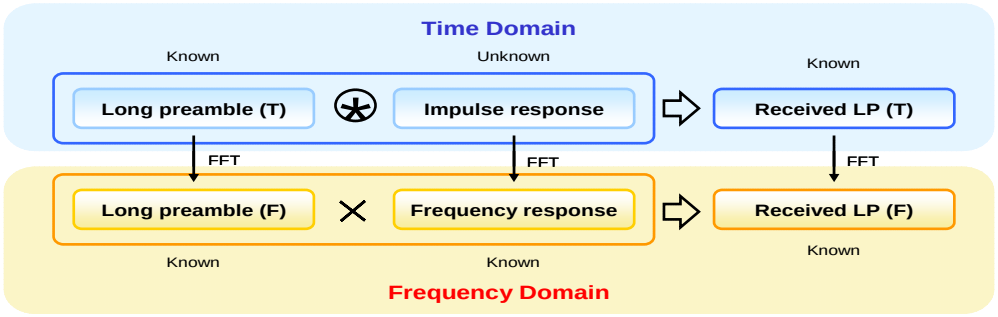

Figure 3.5: Preamble-aided channel estimation scheme

- Pilot-aided channel estimation: Pilot-aided channel estimation is based on LS criteria together with channel interpolation based on piecewise-linear interpolation method. The pilot arrangement of WiMAX systems is comb-type pilot arrangement. The estimate of pilot signals in the *s*th OFDM symbol based on LS criterion is given by

$$H_{Pilot,s} = [H_{Pilot,s}(1)H_{Pilot,s}(2)...H_{Pilot,s}(N_p)] = [\frac{R_{s,1}}{P_{s,1}}\frac{R_{s,2}}{P_{s,2}}\cdots\frac{R_{s,N_p}}{P_{s,N_p}}] \quad (3.15)$$

where $P_{s,l}$ denotes the known N_p pilot signals in the *s*th OFDM symbol and $R_{s,l}$ represents the pilot subcarriers in the *s*th received symbol after taking FFT, l = 1, 2, …, N_p. After the estimation of the channel frequency response of pilot subcarriers, the channel response of data subcarriers can be interpolated according to adjacent pilot subcarriers. Piecewise-linear polynomial interpolation method is used here. Two successive pilot subcarriers are used to determine the channel response in between the pilot subcarriers. For data subcarrier k, $(j-1)M < k \le jM$, the estimated channel response is given by

$$H_{\text{int}erp,s}(k) = H_{Pilot,s}(j) + \frac{m}{M}(H_{Pilot,s}(j+1) - H_{Pilot,s}(j)), 0 \le m < M \quad (3.16)$$

where M is the number of data subcarriers in between the adjacent pilot subcarriers and j = 1, 2, …, N_p. The process of pilot-aided channel estimation is illustrated in Figure 3.6.

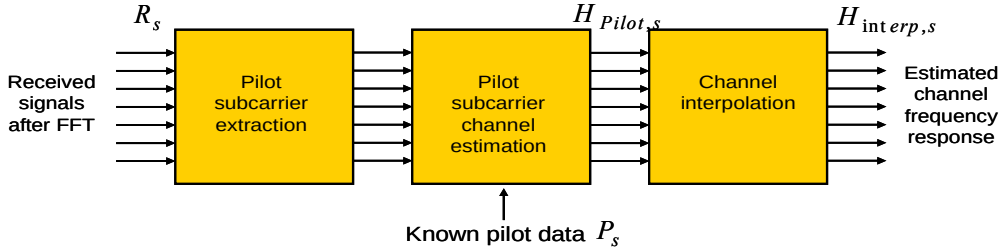

Figure 3.6: Pilot-aided channel estimation scheme

3.4 Phase Estimation

Phase estimation can be regarded as a remedy after over-compensating the received signals by estimated frequency offset mentioned in Section 3.2 [24], [27]. The pilot subcarriers embedded in the data symbol can be used to estimate the rotating phase due to the residual frequency offset. The phase estimator can be expressed as

$$q_s = \sum_{k=pilot\_subcarrier\_index} \left(\hat{H} \cdot P_k(s) \right)^* R_k(s) = Y_s e^{j2\pi\Delta f_r s T_b} \tag{3.17}$$

where $P_k(s)$ represents the known pilot data at the kth subcarrier in the sth OFDM symbol, $\hat{H}$ is the channel estimate of preamble in the frequency domain, $R_k(s)$ represents the received data at the kth subcarriers in the sth OFDM symbol, and T_b and Δf_r denote one symbol time and the residual frequency offset respectively. If there is any residual frequency offset, it is reflected in the phase estimator and we can obtain the rotating phase as $\hat{\phi}_s = \arg\{q_s\} = 2\pi\Delta f_r s T_b$. Therefore, we may have the information for phase tracking on a symbol-by-symbol basis. Furthermore, the residual frequency can be estimated easily via the phase estimator. According to q_s, q_{s+1}, q_{s+2}, …, q_{s+L-1}, the residual frequency Δf_r can be determined as follows:

$$\Delta f_r = \frac{1}{2\pi T_b} \angle \left\{ \sum_{l=1}^{L-1} q_{s+(l-1)}^* q_{s+l} \right\} \tag{3.18}$$

where L denotes the number of symbols in a frame. After the residual frequency is compensated, we can perform channel estimation again to obtain the more accurate channel estimates.

Figure 3.7 shows the MSE of the residual frequency offset estimate as a function of E_b/N_0 in a SISO-OFDM system. The channel model used in this simulation is SUI-3 channel. Compared with the frequency offset estimation method mentioned in Section 3.2, the residual frequency offset estimation method provides better accuracy of

estimation. However, the frequency offset estimation method mentioned in Section 3.2 trades accuracy for a wider range of estimation. So the residual frequency offset estimation method can co-work with the frequency offset estimation method to obtain a wider range and better accuracy of estimates.

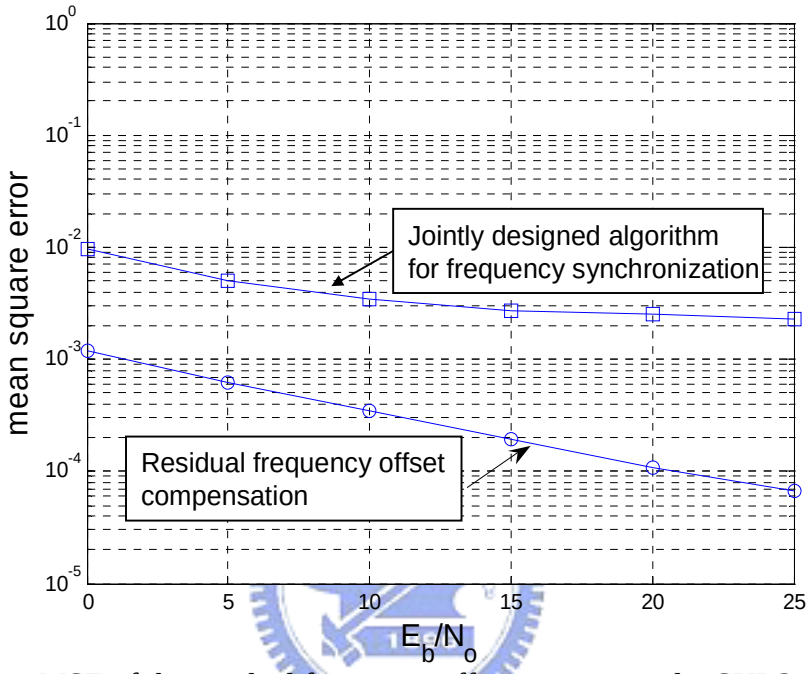

Figure 3.7: MSE of the residual frequency offset estimate under SUI-3 channel model

3.5 Summary

In this chapter, we first introduce two channel models: the first is SUI channel model which is used to form a set of channel models suitable for IEEE 802.16 fixed wireless applications and the second is ITU channel model which is used for mobile wireless applications. After that, we introduce the requirement tasks at the receiver. Synchronization is first introduced and we propose a joint design of timing and frequency synchronization algorithm to lower the computational complexity. Then, channel estimation, phase estimation and residual frequency offset estimation are introduced in the rest part of the receiver. Furthermore, we compare the MSE of the frequency offset estimates after performing residual frequency offset estimation.

Computer simulations of the overall system will be showed in Chapter 4 and the proposed algorithms can work as expected.

The receiver functional blocks that are introduced in this chapter are basic blocks. In order to adapt to different modes, some receiver functional blocks require to be modified. All the modification and more detailed experimental results will be given in Chapter 4.

Chapter 4

SC-OFDM-OFDMA SDR Architecture

Wireless communication standards are evolving rapidly. WiMAX now is an emerging suite of air interface standards for combined fixed, portable and mobile broadband wireless access. To meet the requirements of different standards, SDR technologies enable dynamic reconfiguration on the same platform and minimize the hardware variants. In this chapter, we propose a SC-OFDM-OFDMA SDR system to support the various air-interface standards specified by IEEE 802.16-2005 in a single SDR system. In this way, the system possesses as many common components as possible for these three modes, and the transmitter and receiver can be switched among the three modes via SDR operation. The rest of this chapter is organized as follows. Concept of SDR will be described in Section 4.1. The transmitter architecture of the proposed SC-OFDM-OFDMA SDR system will be introduced in Section 4.2. The receiver architecture of the proposed SC-OFDM-OFDMA SDR system will be introduced in Section 4.3. Finally, computer simulations for different modes and different transmit techniques are shown in Section 4.4.

4.1 Concept of Software Defined Radio

A lot of standards of communication systems have been proposed due to an exponential growing of demands for communications since early 1980. Commercial wireless communication industry is currently facing problems due to constant evolution of link-layer protocol standards (2.5G, 3G, WiMAX, and 4G), existence of incompatible wireless network technologies in different countries inhibiting deployment of global roaming facilities and problems in rolling-out new services/features due to wide-spread presence of legacy subscriber handsets. Therefore this prompts the development of the SDR concept as a potential practical solution. There are several differing definitions of SDR technology. Most commonly it defines a software implementation of the user terminal that is able to dynamically adapt to the radio environment in which it is located time by time.

Over the last few years, analog radio systems are being replaced by digital radio systems for various radio applications in commercial and military spaces. In addition to those, programmable hardware is increasingly being used in many digital radio systems at different level. SDR technology can take these advantages to build an open-architecture software and hardware platform [17], [18], [19].

SDR technology facilitates implementation of some of the functional modules by software in the MAC and PHY layers. This helps in building reconfigurable software radio systems where dynamic selection of parameters for some software-defined functional modules is possible. Also, the software-defined functional modules can be easily updated or upgraded as enhancements to deal with various multi-standard and multi-band architectures.

Although the exact and strict definitions of SDR technology do not yet exist, the following are the key features of SDR technology found in some literature [20], [21]:

- **Reconfigurability:** SDR allows co-existence of multiple software-defined functional modules implementing different standards on the same platform allowing dynamic configuration by just selecting the appropriate parameters for software- defined modules to accommodate new functions and algorithms. The wireless network infrastructure can reconfigure itself to subscriber's handset type or the subscriber's handset can reconfigure itself to network type. SDR technology facilitates implementation of future-proof, multi-service, multi-mode, multi-band, multi-standard terminals and infrastructure equipment.
- **Ubiquitous Connectivity:** SDR enables implementation of air interface standards as software modules and multiple instances of such modules that implement different standards can co-exist in infrastructure equipment and handsets. If the terminal is incompatible with the network technology in a particular region, an appropriate software-defined functional module requires to be installed onto the handset (possibly over-the-air) resulting in seamless network access across various geographies.

Software-defined radio is a future-proof solution to making wireless communication systems highly flexible. The flexibility offered by SDR systems helps in cutting the R&D cost and shortening the time-to-market. Fewer variants mean much lower maintenance and module improvement efforts.

Development of a complete SDR system requires many skill-sets in areas such as RF design, firmware, DSP software, Operating systems, data communication protocols and more. The compatibility of an SDR system is guaranteed by its reconfigurability by DSP engine re-programmability, which implements radio interface and upper layer protocols in real time. It is important to note that DSP is really intended the concept of digital signal processing, and not only DSP chipsets in strict sense, but also field programmable gate arrays (FPGA).

At present, the SDR technology is being actively researched due to its potential to help realize reconfigurable radio systems while retaining common hardware platforms. In this thesis, we will adopt the concept of SDR technology to develop a reconfigurable transceiver architecture for SC-OFDM-OFDMA system based on IEEE 802.16-2005 standard.

4.2 SC-OFDM-OFDMA SDR System: Transmitter Architecture

The block diagram shown in Figure 4.1 represents the transmitter architecture of the proposed SC-OFDM-OFDMA SDR system. In the following section, we will introduce some functional blocks of the transmitter architecture that are modified to be reconfigurable. Here, we will not introduce some functional blocks in detail that have been described in Chapter 2.

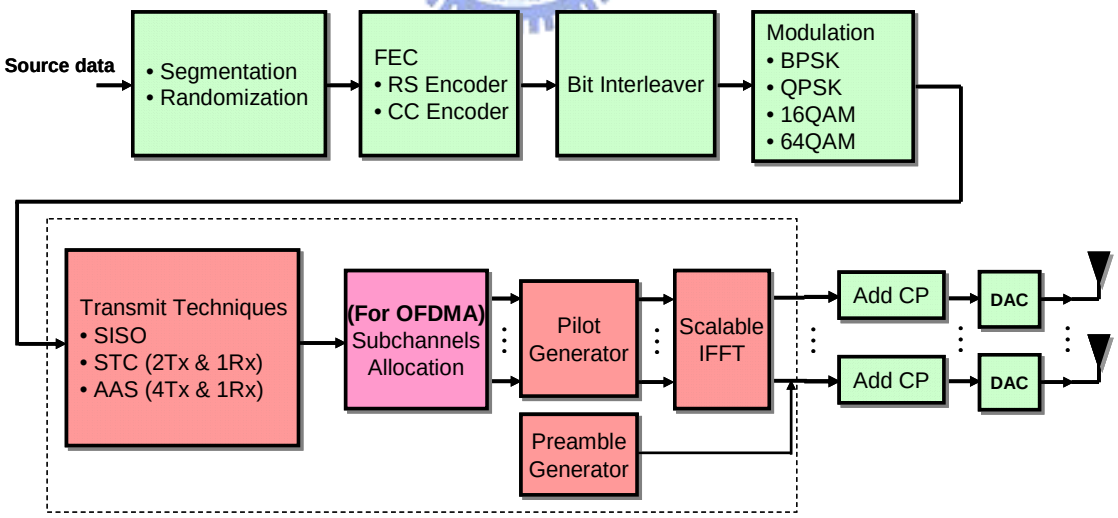

Figure 4.1: Proposed SC-OFDM-OFDMA SDR transmitter architecture

As shown in Figure 4.1, the uncoded data is generated from a random source, consists of a series of zeros and ones. First, the uncoded data shall be passed to a

randomizer. Randomization is performed on each allocation, which means that for each allocation of a data block. After performing randomization, the randomized data shall be passed through the FEC block. The FEC block is performed by first passing the data in block format through the RS encoder and then passing it through the zero-terminating convolutional encoder. It is worthy of mention that the randomized data needs not first pass to the RS encoder in OFDMA transmission mode. After encoding, all encode data shall be interleaved by a block interleaver. After bit interleaving, the data bits are entered serially to the modulator and then mapped to form symbols. Modulation schemes used here are BPSK, QPSK, 16QAM, and 64QAM with gray coding in the constellation map. After constellation mapping, the modulated data will be processed by different transmit techniques such as SISO, STC, and AAS. But the different transmit techniques do not affect the data block size. The data block size is determined by the FEC block, modulator, and the number of subchannels allocated. In the following paragraphs, we will introduce the procedures to determine the uncoded data block size for different modes.

Single Carrier

In SC transmission mode, the receiver will perform frequency domain equalizer by utilizing the *N*-point FFT and IFFT. In order to adapt to the input size of FFT, the transmitter requires performing uncoded data block segmentation. In addition to the FFT size, we still require considering the FEC block and modulator. Under the whole consideration, the uncoded data block size per symbol can be written as

$$\textit{Uncoded data block size} = (N \times m \times c - p) - 2 \times t \tag{4.1}$$

where N denotes the FFT size, m is modulation order (QPSK: m=2, 16QAM: m=4), c is the code rate of CC encoder, p is the number of zero tail bits before CC encoder, and t is the number of data bits which can be corrected after RS encoder. As shown in Table 4.1, the FFT size is specified by 256 and each frame contains 10 symbols. The uncoded

data block size can be easily obtained by equation (4.1) in SC transmission mode.

Table 4.1: Uncoded data block size for SC mode

	QPSK	16QAM
Uncoded block size	208x10 (bits)	432x10 (bits)
RS code	(240,208,16)	(496,432,32)
RS encoded data	240x10	496x10
CC code rate	1/2	1/2
CC encoded data	512x10	1024x10
Modulated data	256x10	256x10

OFDM

In OFDM transmission mode, the mandatory FEC block consists of the concatenation of a Reed-Solomon outer code and a rate-compatible Convolutional inner code. The RS-CC coding rate 1/2 shall always be used as the coding mode when requesting access to the network and in the FCH burst. The FFT size is fixed to be 256 in OFDM transmission mode, consisting of 192 data subcarriers and 8 pilot subcarriers per symbol. In order to achieve the desired overall code rate, the RS encoder and CC code rate require adjustments. The uncoded data block size per symbol can be computed as

$$Uncoded\ data\ block\ size = (192 \times m \times c - p) - 2 \times t \quad (4.2)$$

where m is modulation order (BPSK: m=1, QPSK: m=2, 16QAM: m=4), c is the code rate of CC encoder, p is the number of zero tail bits before CC encoder, and t is the number of data bits which can be corrected after RS encoder. ‘192’ represents the total number of data subcarriers. Table 4.2 gives the uncoded block sizes used for different modulations to achieve overall coding rate 1/2. In the case of BPSK modulation, the RS

encoder should be bypassed. When subchannelization is applied in the uplink, the FEC will bypass the RS encoder and the uncoded data block size can be computed by the number of allocated subchannels divided by 16 (total number of subchannels).

Table 4.2: Uncoded data block size for OFDM-256 mode

	BPSK	QPSK	16QAM
Uncoded block size	80x10 (bits)	176x10 (bits)	352x10 (bits)
RS code	(80,80,0)	(240,176,32)	(480,352,64)
RS encoded data	80x10	240x10	480x10
CC code rate	1/2	2/3	2/3
CC encoded data	192x10	384x10	768x10
Modulated data	192x10	192x10	192x10
Overall coding rate	1/2	1/2	1/2

OFDMA

In OFDMA transmission mode, the mandatory coding scheme is convolution encoder. The encoding block size will depend on the modulation order and the number of subchannels allocated for the current transmission. As mentioned in Chapter 2, each subchannel is composed of 24 data subcarriers and 4 pilot subcarriers for PUSC permutation. According to the number of subchannels allocated and code rate, the uncoded data block size per symbol can be derived as

$$Uncoded\ data\ block\ size = N_{sc} \times 24 \times 2 \times m \times c - p \quad (4.3)$$

where N_{sc} denotes the number of subchannels allocated, m is modulation order (QPSK: m=2, 16QAM: m=4, 64QAM: m=6), c is the code rate of CC encoder, p is the number of zero tail bits before CC encoder, and '2' represents the number of spanned symbols for a slot in downlink PUSC. Although the FFT size can be scaled to adapt to different channel bandwidths in OFDMA mode, different FFT sizes still use the same equation (4.3) to determine the uncoded data block size. The uncoded data block sizes

for different FFT sizes are shown in Tables 4.3, 4.4, 4.5 and 4.6. The four tables provide the overall coding rate 1/2 in the case with the whole subchannels allocated in Major Group 0. The total number of subchannels in Major Group 0 is specified in Table 4.7 for different FFT sizes.

Table 4.3: Uncoded data block size for OFDMA-2048 mode

	QPSK	16QAM	64QAM
Uncoded block size	560x5 (bits)	1136x5 (bits)	1712x5 (bits)
CC code rate	1/2	1/2	1/2
CC encoded data	1152x5	2304x5	3456x5
Modulated data	576x5	576x5	576x5
Overall coding rate	1/2	1/2	1/2

Table 4.4: Uncoded data block size for OFDMA-1024 mode

	QPSK	16QAM	64QAM
Uncoded block size	272x5 (bits)	560x5 (bits)	848x5 (bits)
CC code rate	1/2	1/2	1/2
CC encoded data	576x5	1152x5	1728x5
Modulated data	288x5	288x5	288x5
Overall coding rate	1/2	1/2	1/2

Table 4.5: Uncoded data block size for OFDMA-512 mode

	QPSK	16QAM	64QAM
Uncoded block size	224x5 (bits)	464x5 (bits)	704x5 (bits)
CC code rate	1/2	1/2	1/2
CC encoded data	480x5	960x5	1440x5
Modulated data	240x5	240x5	240x5
Overall coding rate	1/2	1/2	1/2

Table 4.6: Uncoded data block size for OFDMA-128 mode

	QPSK	16QAM	64QAM
Uncoded block size	32x5 (bits)	80x5 (bits)	128x5 (bits)
CC code rate	1/2	1/2	1/2
CC encoded data	96x5	192x5	288x5
Modulated data	48x5	48x5	48x5
Overall coding rate	1/2	1/2	1/2

Table 4.7: Number of subchannels in Major Group 0 for different FFT sizes

FFT size	PUSC Downlink			
	Total useful subcarriers (DC,pilot,data)	Total pilots	Subchannels in Major Group 0	Data subcarriers per subchannel
128	85	12	1	24
512	421	60	5	24
1024	841	120	6	24
2048	1681	240	12	24

Once the uncoded data block size is decided and the uncoded data is encoded and modulated, the pilot subcarriers shall be inserted into each data block in order to constitute a symbol and they shall be modulated according to their locations within a symbol. The first symbol of the downlink transmission is the preamble. In OFDM and OFDMA transmission mode, each symbol will be fed into IFFT and transmitted in different formats by using various transmit techniques such as STC and AAS. SC transmission mode will bypass the IFFT block. Here, we omit the detail descriptions of other blocks that have been introduced in Chapter 2.

4.3 SC-OFDM-OFDMA SDR System: Receiver Architecture

System scalability is a key design consideration in the development of the SDR system. The proposed SC-OFDM-OFDMA system requires modification of algorithms in order to accommodate various air interfaces. The proposed SDR receiver involves many blocks shown in Figure 4.2. Here, we focus on three blocks, such as timing and frequency synchronization block, channel estimation block, and phase estimation block. These three common algorithms will be designed to match the functionality of the prescribed air interfaces by setting suitable parameters.

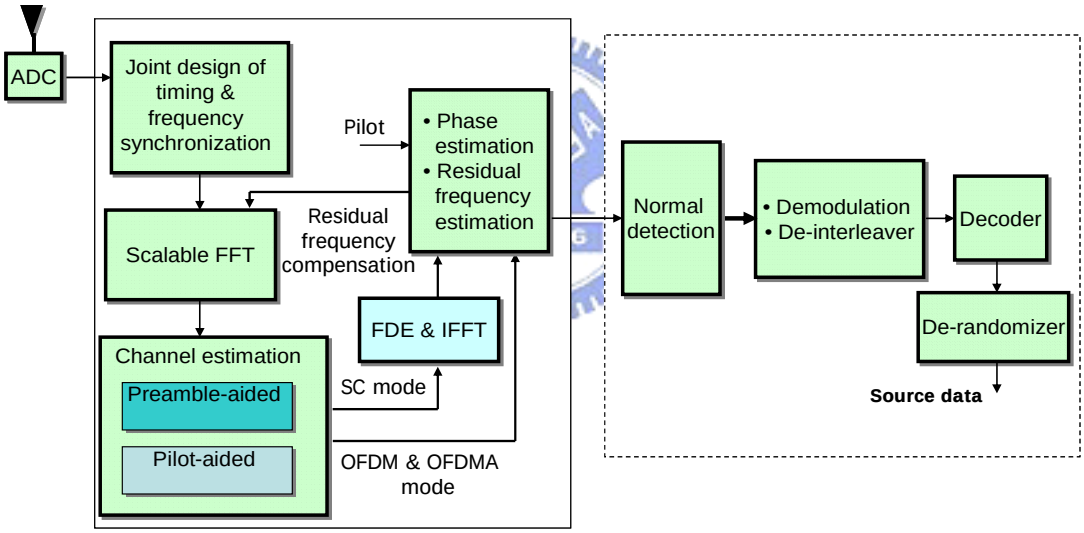

Figure 4.2: Proposed SC-OFDM-OFDMA SDR receiver architecture

4.3.1 Timing and Frequency Synchronization Block

As mentioned in Section 3.2, we have introduced the proposed joint design algorithm of timing and frequency synchronization by utilizing the short preamble [26], [27]. Unfortunately, the short preamble is not always transmitted in any mode. Based on the IEEE 802.16-2005 standards, we can find that only OFDM and SC mode transmit the short preamble preceding the long preamble. In other modes such as

OFDMA mode or modes in which AAS or STC is employed, the preamble structure only consists of a long preamble. In order to adapt to different modes in the SDR system, the jointly designed algorithm of timing and frequency synchronization should be modified in order to obtain the reliable timing and frequency offset estimates.

The operation of timing and frequency synchronization by using the short preamble is the same as Section 3.2. The preamble structures can be classified into two cases:

case Ⅰ: the case with short preambles; case Ⅱ: the case without short preambles

Here, we modify the metrics slightly to perform timing and frequency synchronization correctly in case Ⅱ. The preamble structure of a long preamble with CP is shown in Figure 4.3. Unlike the four repetitions of short preamble, we can find that CP is the only repetition part of the preamble structure as seen in Figure 4.3. So we can use CP to perform timing and frequency synchronization.

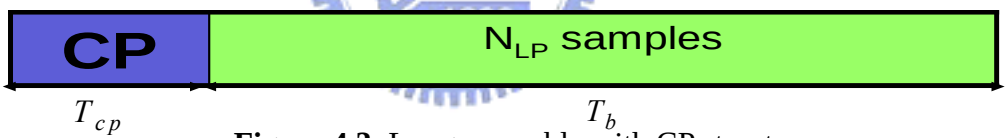

Figure 4.3: Long preamble with CP structure

In the following paragraphs, we will explain how to adjust the parameters to accommodate the two schemes step by step.

- Step 1: *Adjust the window size and shift width and compute the delay correlation outputs*

  The delay correlation outputs can be obtained by correlating the received signal and the known preamble over a window of *v* samples. The delay correlation outputs ψ_L and ψ_R of the *i*th received samples can be written as

$$\psi_{L,n}(i) = \sum_{k=0}^{v-1} \left(s_L^* \cdot r_{i+(n-1)\cdot f+k} \right)$$

$$\psi_{R,n}(i) = \sum_{k=0}^{v-1} \left(s_R^* \cdot r_{i+(n-1)\cdot f+k+v} \right) \tag{4.4}$$

where s_L and s_R denote the {1,v} and {v+1,2×v} samples. In case Ⅰ, s_L and s_R belong to short preamble. In case Ⅱ, s_L and s_R belong to CP. Here, the CP length is configured to be 1/4 of the FFT length for simplicity. v represents the window size for summing up the correlation outputs. It is set to be 32 in case Ⅰ, and set to be half of the CP length in case Ⅱ. f represents the shift width for the next delay correlation output starting point. It is set to be 64 in case Ⅰ. In case Ⅱ, the spacing of CP and its replica equal FFT length. n is the index of delay correlation outputs for the ith received samples. n equals 1,2,3, and 4 in case Ⅰ, and equals 1 and 2 in case Ⅱ. There are $2 \cdot \max(n)$ delay correlation outputs that will be stored for each received samples. The operations of computing delay correlation outputs in case Ⅰ and case Ⅱ are shown in Figures 4.4 and 4.5 respectively.

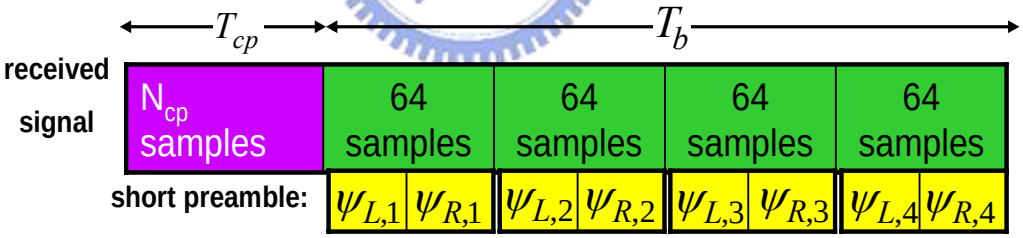

Figure 4.4: Operation of computing delay correlation outputs in the case with short preamble

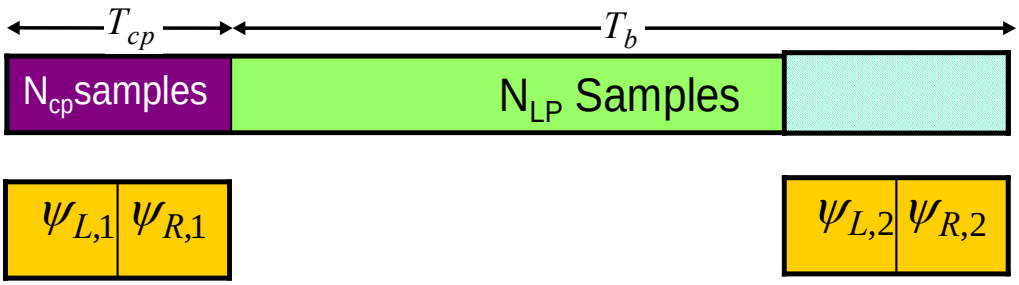

Figure 4.5: Operation of computing delay correlation outputs in the case without short preamble

- Step 2: *Use the delay correlation outputs to perform timing synchronization*

After collecting groups of *2n* delay correlation outputs obtained in Equation (4.4), the best timing instant can be detected by choosing the peak value of $\Psi(i)$ which is computed by

$$\Psi(i) = \sum_{n=1}^{z/2} \left|\psi_{R,n}(i)\right|^2 + \sum_{n=1}^{z/2} \left|\psi_{L,n}(i)\right|^2 , \tag{4.5}$$

where $\Psi(i)$ represents the timing acquisition metric, and z is the number of delay correlation outputs for the ith received samples and equals 8 in case Ⅰ and equals 4 in case Ⅱ. Once the best starting position of the received signal is detected, frequency synchronization can then be performed.

- Step 3: *Use the corresponding delay correlation outputs to perform frequency synchronization*

The frequency offset is estimated by choosing the delay correlation outputs that produce a peak value in $\Psi(i)$. Hence a frequency offset estimate can be found based on the phase of the delay correlation outputs as follows:

$$\begin{aligned} \Delta f &= \frac{1}{2\pi T} \angle\left\{\phi_{d_{opt}}\right\} \\ &= \frac{1}{2\pi T} \angle\left\{ \sum_{n=1}^{z/2-1} \psi_{L,n}(i)\psi_{L,n+1}^{*}(i) + \sum_{n=1}^{z/2-1} \psi_{R,n}(i)\psi_{R,n+1}^{*}(i) \right\} \end{aligned} \tag{4.6}$$

where T is the duration of the short preamble in case Ⅰ and the symbol time in case Ⅱ. d_{opt} is the optimum timing acquisition instant, and z is the number of delay correlation outputs for the ith received samples.

According to the aforementioned parameter adjustments, the SDR receiver architecture can be easily synchronized with received signal over different air interfaces without making changes to the hardware platform.

4.3.2 Channel Estimation Block

In section 3.3, we have described two channel estimation schemes to deal with different environments. Preamble-aided channel estimation is suited for low-speed applications. For vehicular speed applications, retraining the channel estimate by periodically inserting a midamble seems to resist the time varying channel. However, this scheme will require significant overhead to achieve the pilot-aided scheme performance. All in all, pilot-aided channel estimation scheme performs considerably better than preamble-aided channel estimation for vehicular speed applications and with no additional overhead.

In the case with the pilot-aided channel estimation scheme, the pilot tones are not always in the same location at each symbol for different modes. For OFDM mode, the pilot tones are in the same location at each symbol. For OFDMA mode, the pilot tones are allocated in different location at odd and even symbols. The pilot arrangements have been introduced in Chapter 2. So when performing the pilot-aided channel estimation scheme, the SDR receiver architecture needs to be adapted to different pilot arrangements.

4.3.3 Phase Estimation Block

As mentioned in Section 3.4, there is always some residual frequency error because the frequency estimation is not accurate. The residual frequency offset results in constellation rotation. This is the reason why the receiver has to track the carrier phase after performing frequency synchronization [28].

The pilot subcarriers embedded in the data symbol can be used to estimate the rotating phase due to the residual frequency offset. The phase estimator can be expressed as

$$q_s = \sum_{k=pilot\_subcarrier\_index} \left(\hat{H} \cdot P_k(s) \right)^* R_k(s) = Y_s e^{j2\pi\Delta f_r s T_b} \tag{4.7}$$

where $P_k(s)$ represents the known pilot data at the *k*th subcarrier in the *s*th OFDM symbol, $\hat{H}$ is the channel estimate of preamble in the frequency domain, $R_k(s)$ represents the received data at the *k*th subcarriers in the *s*th OFDM symbol, and T_b and Δf_r denote one symbol time and the residual frequency offset respectively. If there is any residual frequency offset, it is reflected in the phase estimator and we can obtain the rotating phase as $\hat{\phi}_s = \arg\{q_s\} = 2\pi\Delta f_r s T_b$. Therefore, we may have the information for phase tracking on a symbol-by-symbol basis. Furthermore, the residual frequency offset can be estimated easily via the phase estimator. As mentioned in the above, the pilot arrangements are different for the different modes. In OFDM mode, the pilot tones are always in the same location at each symbol. According to q_s, q_{s+1}, q_{s+2}, …, q_{s+L-1}, the residual frequency offset can be determined as follows:

$$\Delta f_r = \frac{1}{2\pi T_b} \angle \left\{ \sum_{l=1}^{L-1} q_{s+(l-1)}^* q_{s+l} \right\} \tag{4.8}$$

where *L* denotes the number of symbols in a frame. In OFDMA mode, the pilot tones are allocated in different location at odd and even symbols. So we divide the phase estimators into two groups and the residual frequency offset can be written as

$$\Delta f_r = \frac{1}{2\pi 2T_b} \angle \left\{ \sum_{l=even} q_{s+(l-2)}^* q_{s+l} + \sum_{l=odd} q_{s+(l-2)}^* q_{s+l} \right\} \tag{4.9}$$

where '*even*' and '*odd*' represent the even numbered and odd numbered symbols respectively. After the residual frequency offset is compensated, we can perform channel estimation again to obtain the more accurate channel estimate.

4.4 Computer Simulations

In this section, computer simulations are conducted to evaluate the performance of the proposed SC-OFDM-OFDMA SDR system. Also, the computer simulations of the proposed SDR system with transmit techniques such as STC and AAS are shown in this section. Throughout the simulations, we only deal with discrete time signal processing in the baseband, hence pulse shaping filter is removed from consideration for simplicity.

Figures 4.6, 4.7 and 4.8 show the proposed SDR receiver architectures for OFDM, OFDMA, and SC transmission mode. As seen in these three figures, it is clearly observed that most functional blocks of the three modes are used commonly. So the proposed SDR receiver can be switched among the three modes via the concept of SDR operation. Figures 4.6, 4.7 and 4.8 also give the parameter adjustments among the three modes.

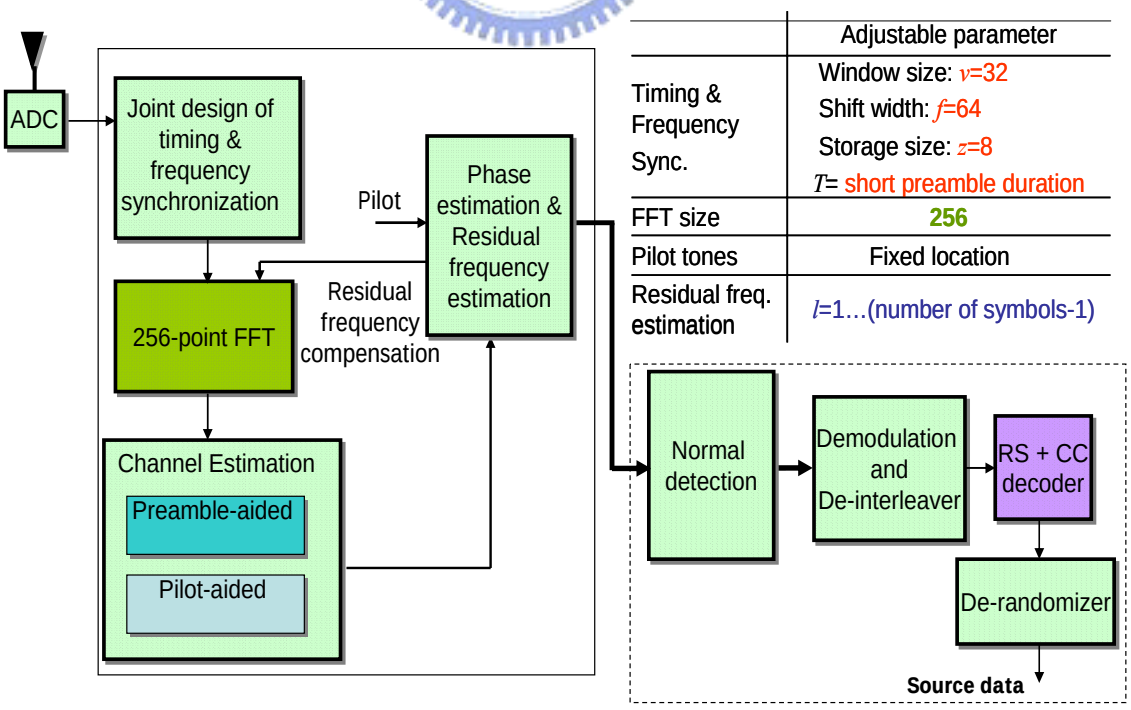

Figure 4.6: SDR receiver architecture for OFDM mode

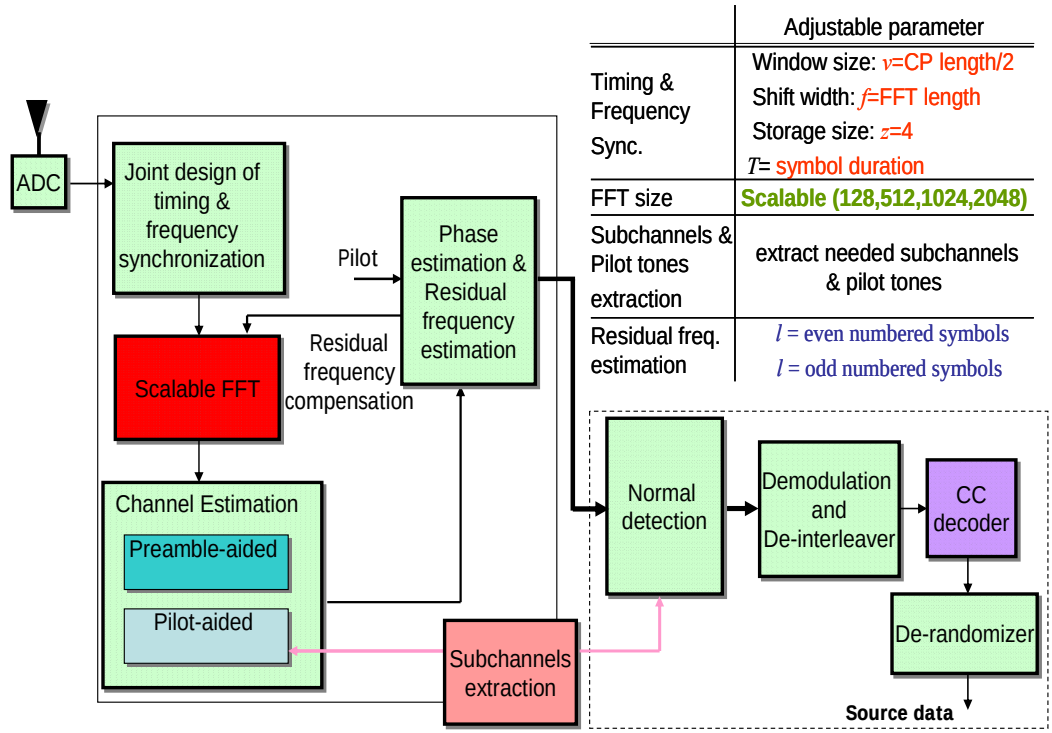

Figure 4.7: SDR receiver architecture for OFDMA mode

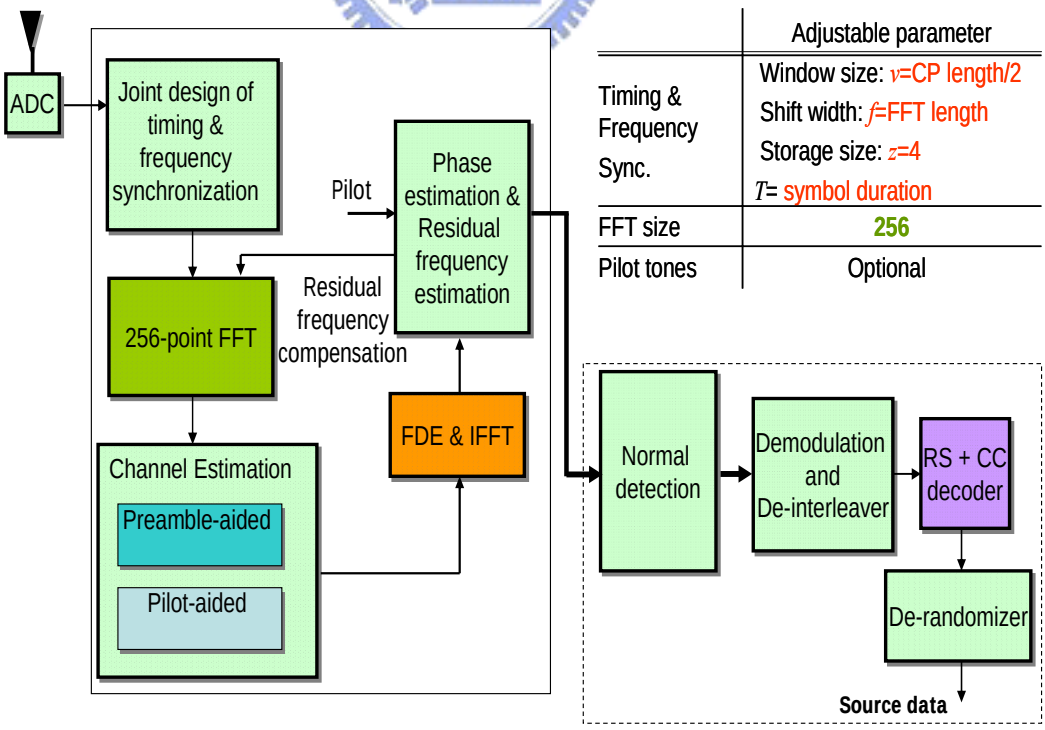

Figure 4.8: SDR receiver architecture for SC mode

In the simulation results, BER performance as a function of E_b/N_0 is evaluated. There is a relation between SNR and E_b/N_0 as follows:

$$SNR = \frac{\text{signal power}}{\text{noise power}} = \frac{E_s \cdot \frac{1}{T_{FFT}}}{N_0 B} = \frac{E_s \cdot \frac{1}{T_{FFT}}}{N_0 \cdot \frac{1}{T_{samp}}} = \frac{E_b}{N_0} \cdot \frac{N_t \cdot M \cdot N_{c\_data}}{N_c} \tag{4.10}$$

where E_s is the symbol energy, N_c is FFT size, T_{FFT} is the symbol duration of the useful part of the received data, T_{samp} is sampling time, N_t is the number of transmit antennas, M equals $\log_2(\text{constellation size of modulation})$, B is the bandwidth of the system, N_{c_data} is the number of data subcarriers, and E_b is the bit energy. If N_{c_data} equals N_c, we can obtain Equation (4.11). Total transmit power is normalized to 1. Hence, we can obtain the relation between noise power and E_b/N_0:

$$\text{noise power} = \frac{1}{\frac{E_b}{N_0} \cdot M \cdot N_t} \tag{4.11}$$

With the consideration of practical implementation, we evaluate the performance impact due to the proposed jointly designed synchronization algorithm and channel estimation algorithm under SUI-1 channel and Vehicular A channel. The parameters of multipath fading channel models for SUI-1 channel and Vehicular A channel are shown in Table 4.8. SUI-1 channel model is mainly used in SC mode. Under Vehicular A channel model, the individual multi-path is subject to the independent Rayleigh fading, whose time domain correlation is implemented by the Jakes model. We also consider the vehicular speeds at 3 km/h and 120 km/h in Vehicular A channel model. All BER are evaluated by averaging over 30000 frames, and each frame has 10 symbols.

Table 4.8: Channel models used in the simulations

	SUI-1 channel K=20,10,0		Vehicular A environment 3km/h,60km/h,120km/h	
Tap	Relative delay (ns)	Average power (dB)	Relative delay (ns)	Average power (dB)
1	0	0	0	0
2	400	–15	310	–1
3	900	–20	710	–9
4	–	–	1090	–10
5	–	–	1730	–15
6	–	–	2510	–20

Table 4.9 lists all parameters used in our simulations. The symbol time and the subcarrier spacing are fixed. The oscillator offset is set to be 5 KHz for carrier frequency at 2.5 GHz. The CP length is chosen as $T_b / 4$ to ensure the maximum delay spread smaller than the CP length, and the modulation schemes used here are BPSK, QPSK, 16QAM and 64QAM. The size of FFT is scaled according to the different bandwidths to keep the subcarrier spacing constant. Table 4.10 gives all the scalability parameters used for the different FFT sizes and bandwidths.

Table 4.9: Simulation parameters for mobile WiMAX

Parameters	**Mobile WiMAX**		
	SISO	**STC**	**AAS**
Number of Transmit/Receive Antennas	**1/1**	**2/1**	**4/1**
Operating Frequency	**2.5 GHz**		
Duplex	**TDD**		
Channel BW	**1.25/2.5/5/10/20 MHz**		
Subcarrier Spacing	**11.16 kHz**		
Useful Symbol Duration/CP Duration	**89.6 μs/22.4 μs (T_b/4)**		
Data Symbols Per Frame	**10**	**8**	**10**
Channel Model	**SUI-1 (for SC)/ ITU VehA 3, 60, 120 km/hr (for other modes)**	**ITU VehA 3,60,120 km/hr**	**ITU VehA 3,60,120 km/hr**

Table 4.10: OFDMA scalability parameters for different bandwidth

Parameters	Values				
Bandwidth (MHz)	**1.25**	**2.5**	**5**	**10**	**20**
Sampling frequency (MHz)	**1.43**	**2.86**	**5.71**	**11.4**	**22.8**
FFT size	**128**	**256**	**512**	**1024**	**2048**
Subcarrier spacing	**11.16 kHz**				
Useful symbol time (Tb)	**89.6 μs**				
CP duration	**22.4 μs (Tb/4)**				

BER performances of the proposed SC-OFDM-OFDMA SDR architecture in OFDM transmission mode are shown in Figures 4.9, 4.10, and 4.11. In these simulations, the size of FFT equals 256 and the system is equipped with a single antenna. In OFDM transmission mode, the short preambles can be used to perform timing and frequency synchronization. It is obviously observed that the BER performance with preamble-aided channel estimation is better than that with pilot-aided channel estimation at 3 km/h under Vehicular A channel model because its number of pilots is not enough to track the channel variation between the two adjacent pilot subcarriers. However, under Vehicular A 120 km/h channel, the performance with pilot-aided channel estimation is superior to that with preamble-aided channel estimation. With pilot-aided channel estimation, the BER curve will be flat at high SNR due to the channel estimation error.

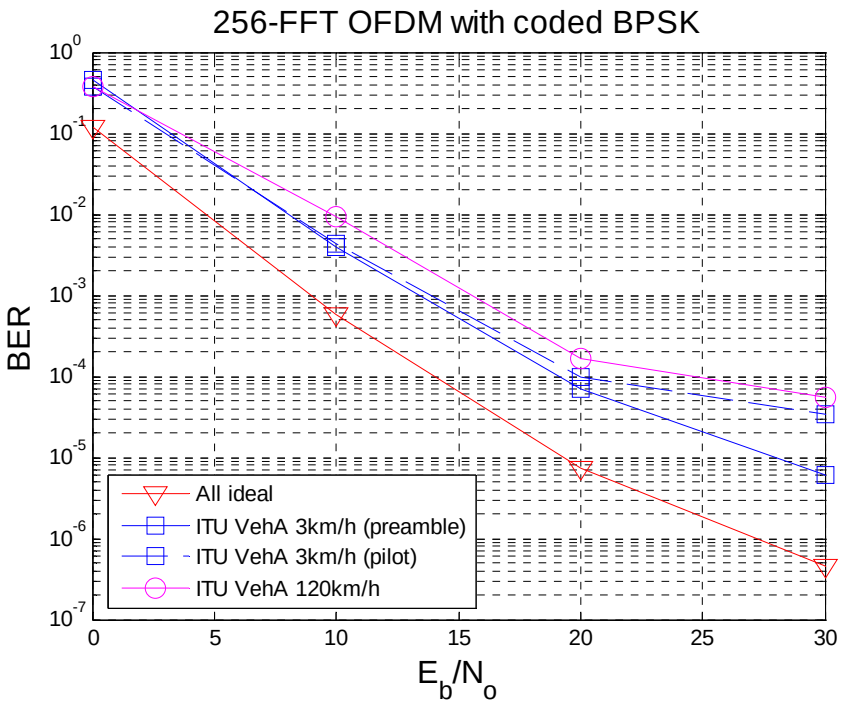

Figure 4.9: BER performance with 256-point FFT with BPSK in OFDM transmission mode under Veh A channel

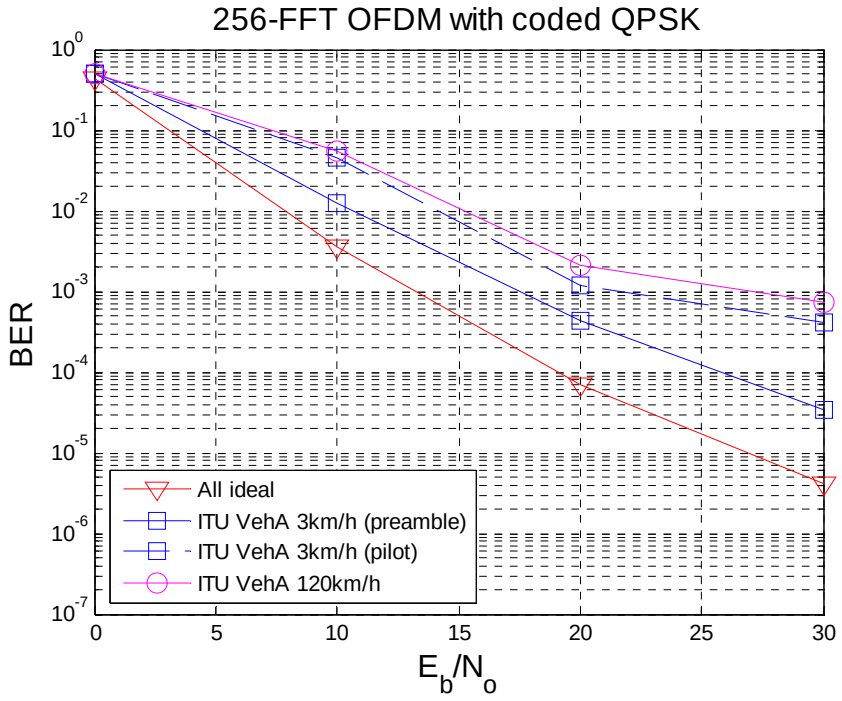

Figure 4.10: BER performance with 256-point FFT with QSPK in OFDM transmission mode under Veh A channel

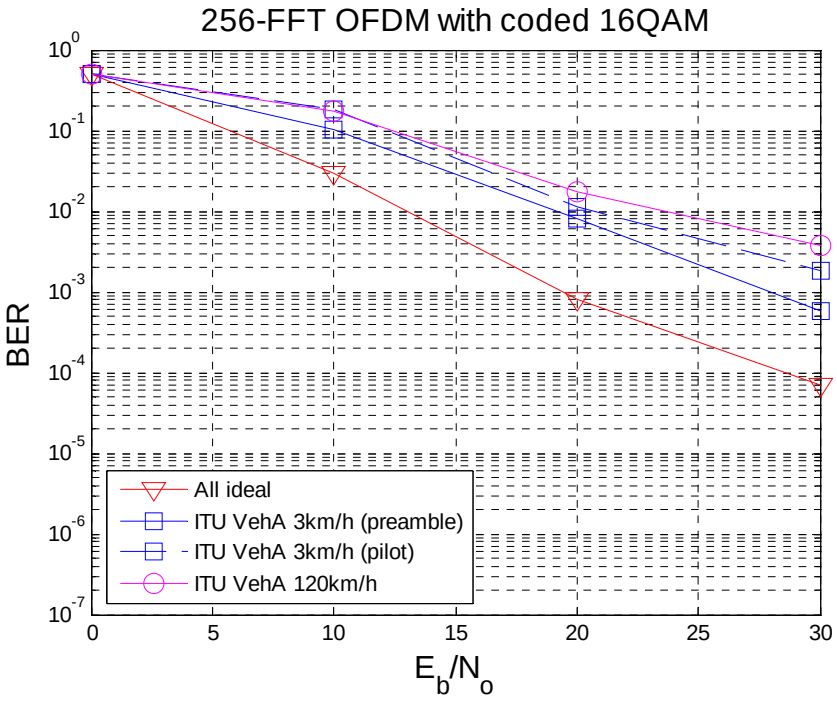

Figure 4.11: BER performance with 256-point FFT with 16QAM in OFDM transmission mode under Veh A channel

BER performances of the proposed SC-OFDM-OFDMA SDR architecture in OFDMA transmission mode are shown in Figures 4.12-4.15. The FFT size in OFDMA transmission mode can be scaled to be 128, 512, 1024, and 2048. In OFDMA transmission mode, the CP can be used to perform timing and frequency offset synchronization. It is worthy of mention that the proposed SDR system keeps the symbol time and subcarrier spacing constant. With these mentioned practical considerations, the overall BER performance of the OFDMA-2048 mode with QPSK will have about 0.3 dB implementation loss compared with the ideal case under Vehicular A 120 km/h channel model. Therefore, with the proposed joint design of synchronization algorithm and the channel estimation algorithm, the proposed SDR system performance has very little degradation compared with the ideal case system. First, the performances of the different FFT sizes are compared. It is observed that from the OFDMA-2048 mode to the OFDMA-128 mode, the performance loss compared

with the ideal case becomes larger and larger (from 0.3 dB to 5 dB as BER=0.001). It's found that the OFDMA-128 mode performs poorest than other FFT sizes because its CP length is too short to estimate the frequency offset accurately. Figure 4.16 figures out the MSE of the frequency offset estimate with 128-point, 512-point, 1024-point and 2048-point FFT under the same channel condition. Second, as seen in Figure 4.12, it is obviously observed that the BER curve will be flat due to the timing and frequency offset estimation error. Third, the sample time varies with the different bandwidths. When the FFT size becomes larger, the sample time will become smaller and then make the delay spread larger. In the case with 128-point, 512-point, 1024-point and 2048-point FFT, it can be found that the delay spread which is smaller than the CP length will not degrade the performance although the delay spread becomes larger. Finally, in OFDMA transmission mode, its number of pilot tones is enough so that the two adjacent pilots enable to track the channel variation accurately between the two adjacent pilot subcarriers.

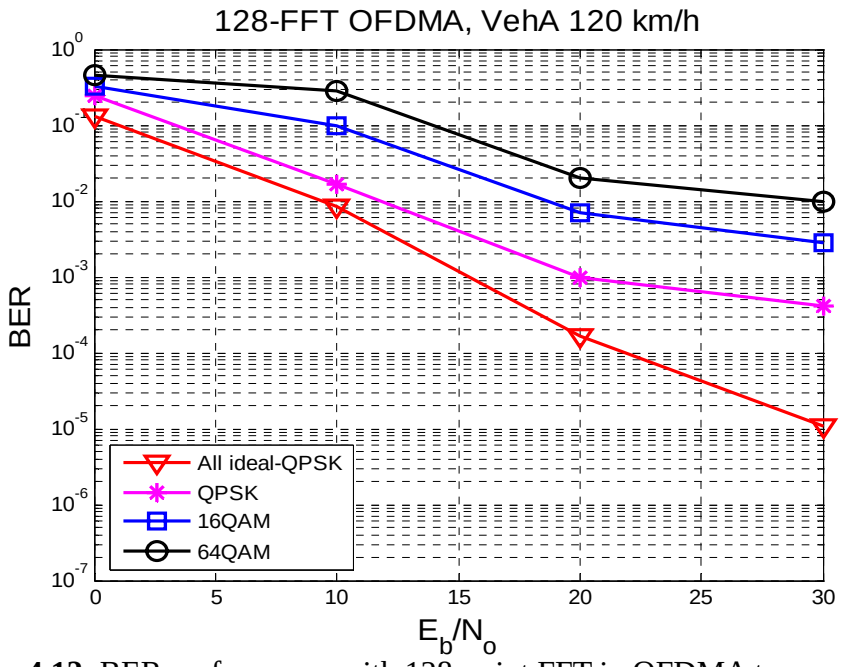

Figure 4.12: BER performance with 128-point FFT in OFDMA transmission mode under Veh A channel

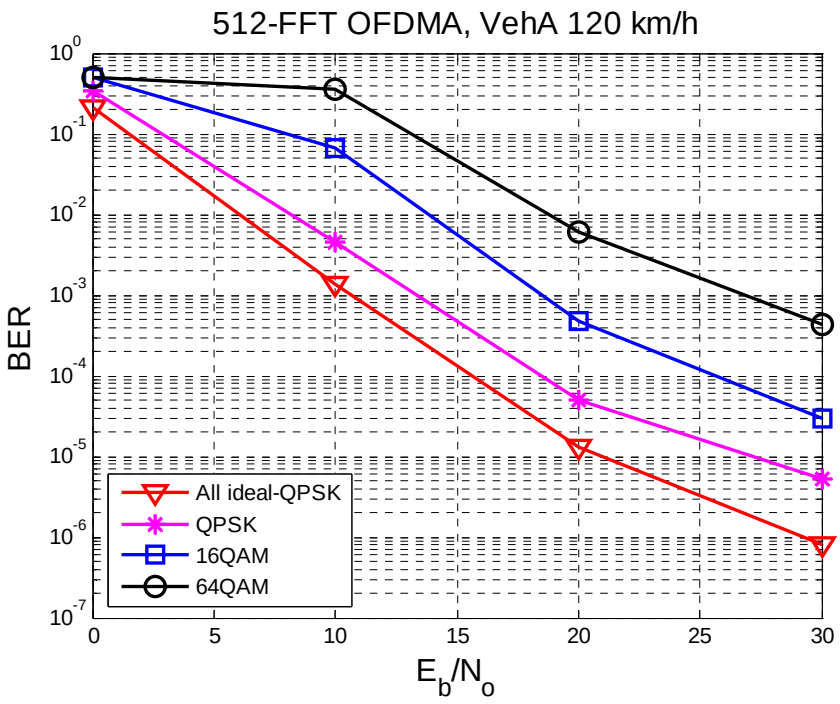

Figure 4.13: BER performance with 512-point FFT in OFDMA transmission mode under Veh A channel

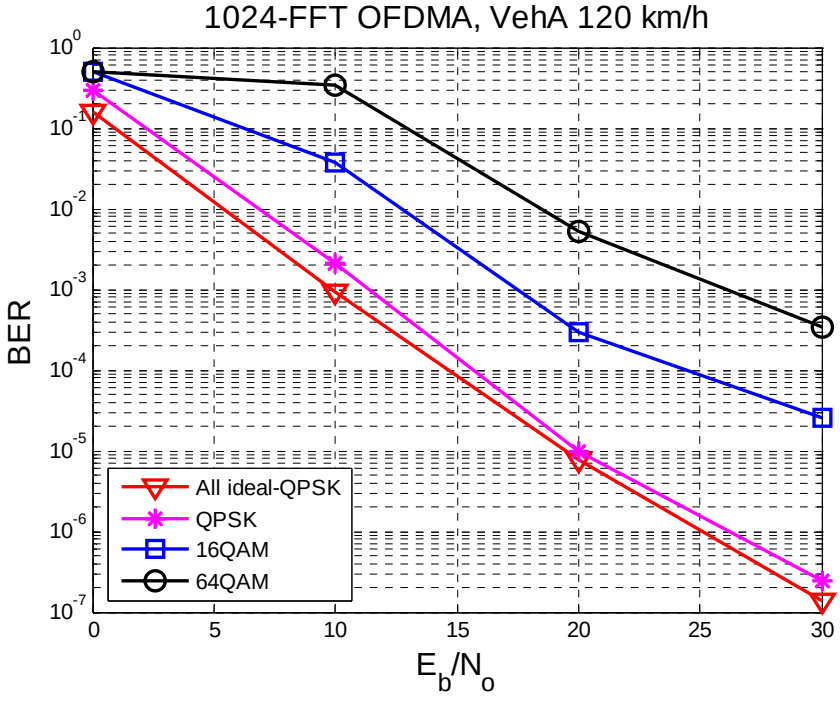

Figure 4.14: BER performance with 1024-point FFT in OFDMA transmission mode under Veh A channel

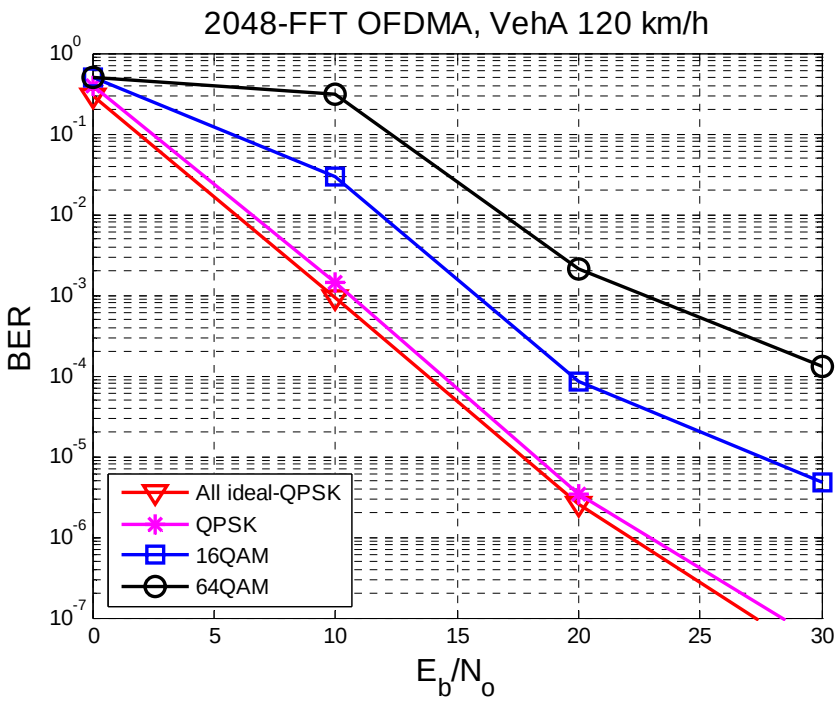

Figure 4.15: BER performance with 2048-point FFT in OFDMA transmission mode under Veh A channel

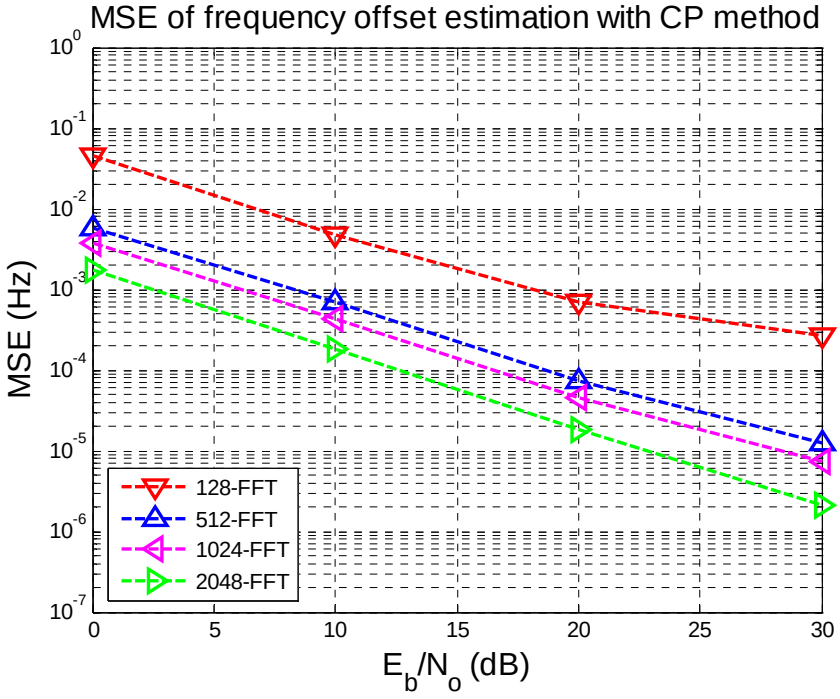

Figure 4.16: MSE of frequency offset estimates in OFDMA-128, 512, 1024 and 2048 mode

BER performances of the proposed SC-OFDM-OFDMA SDR architecture in SC transmission mode are shown in Figures 4.17 and 4.18. SUI-1 channel is used in these simulations and its parameter is shown in Table 4.8. The outer code is RS(240,208,16) for QPSK and RS(496,432,32) for 16QAM and the inner code is CC code rate 1/2. Timing and frequency synchronization schemes are performed by utilizing its CP like the case in OFDMA transmission mode. It is obviously observed that LOS channels with Rice factor K=20 and K=10 are suitable for SC transmission mode. The performance of the case with Rice factor K=0 is poorer because the SC transmission mode is not robust against NLOS environments.

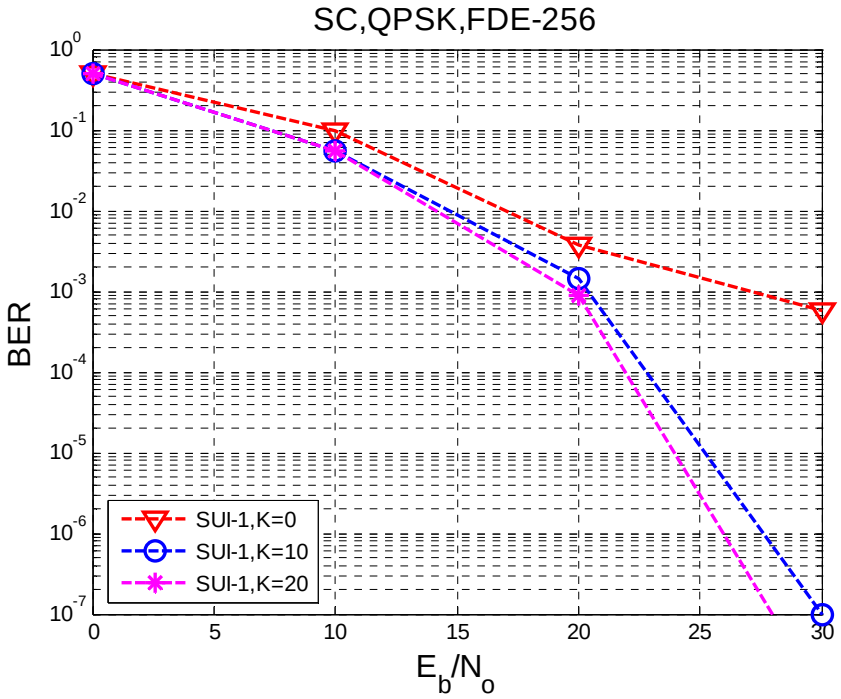

Figure 4.17: BER performance with coded QPSK in SC transmission mode under SUI-1 channel

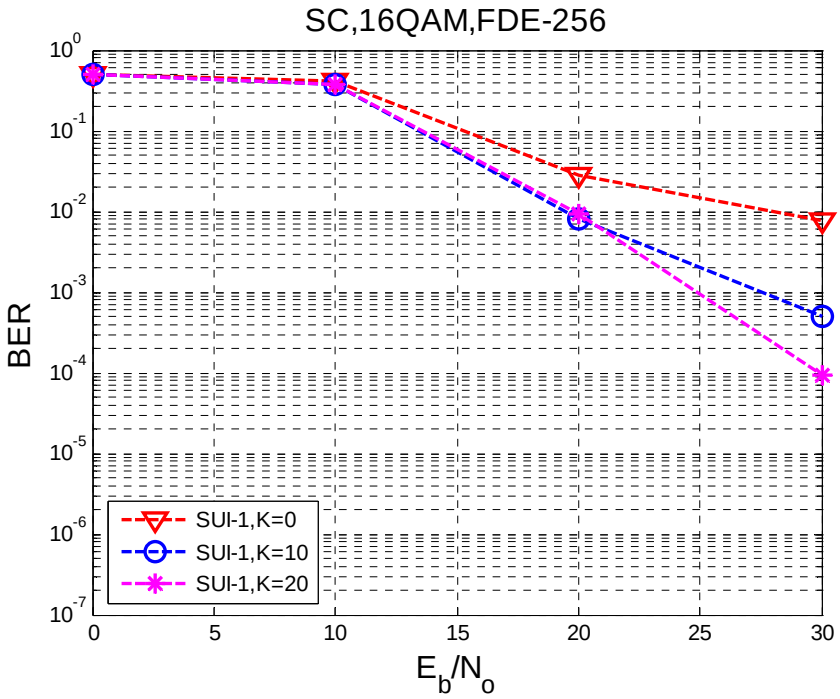

Figure 4.18: BER performance with coded 16QAM in SC transmission mode under SUI-1 channel

Finally, the performances with transmit techniques such as STC and AAS will be verified to exhibit the improved performances. Simulation results with STC are shown in Figures 4.19, 4.20 and 4.21. Under Vehicular A 3 km/h channel environments, STC with two transmit antennas and one receive antenna provides over 5 dB gain than in SISO mode at a bit error rate of 0.0001. With higher vehicular speed, the BER curve will be flat because the time-varying fading rate is too fast. Under Vehicular A 60 km/h channel environments, it is clearly observed that the lower order modulation is more robust against time-varying channel environments.

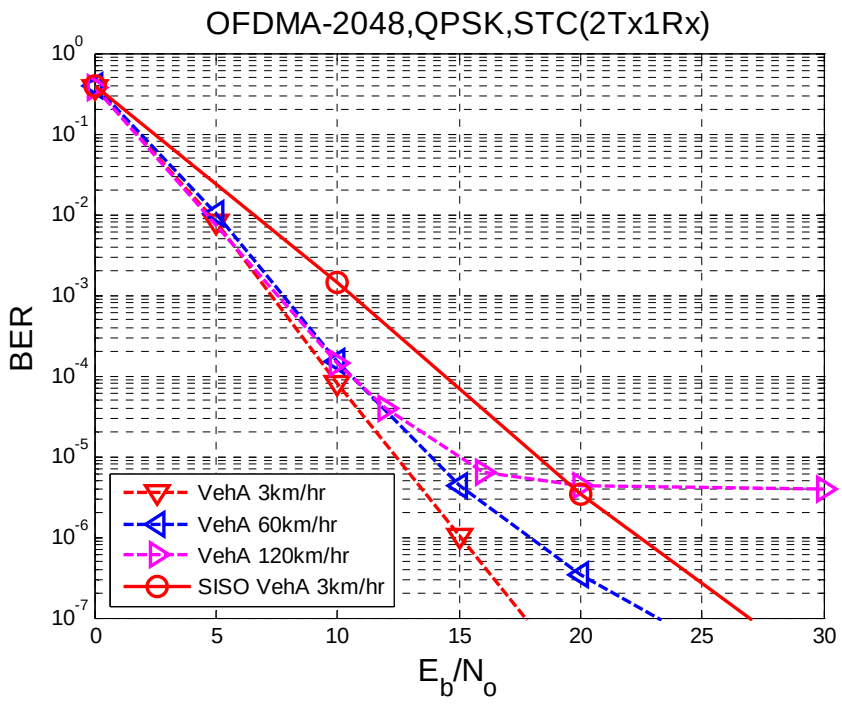

Figure 4.19: BER performance with STC (2Tx1Rx) and QPSK in OFDMA-2048 mode under Veh A channel

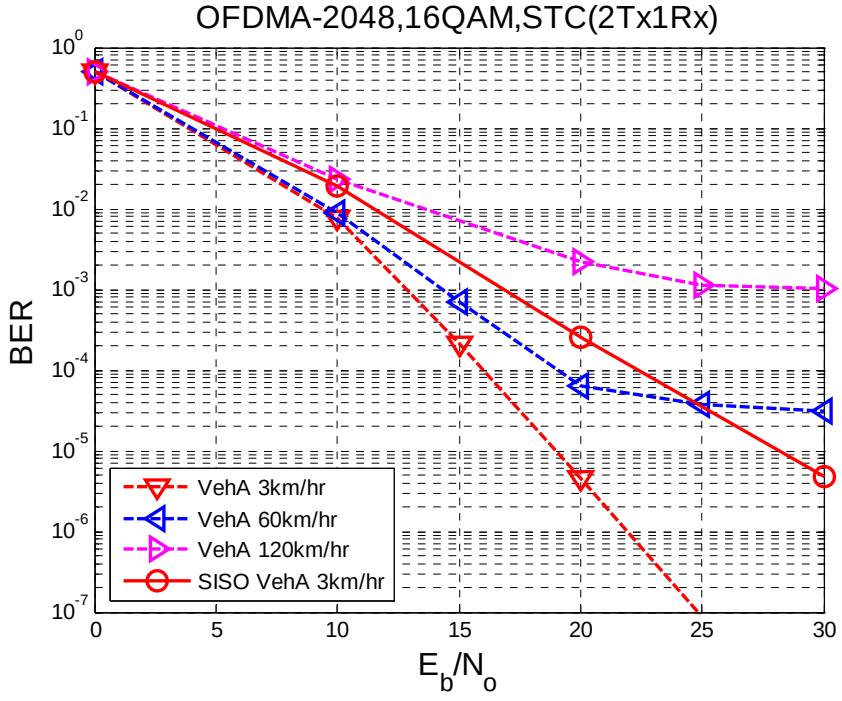

Figure 4.20: BER performance with STC (2Tx1Rx) and 16QAM in OFDMA-2048 mode under Veh A channel

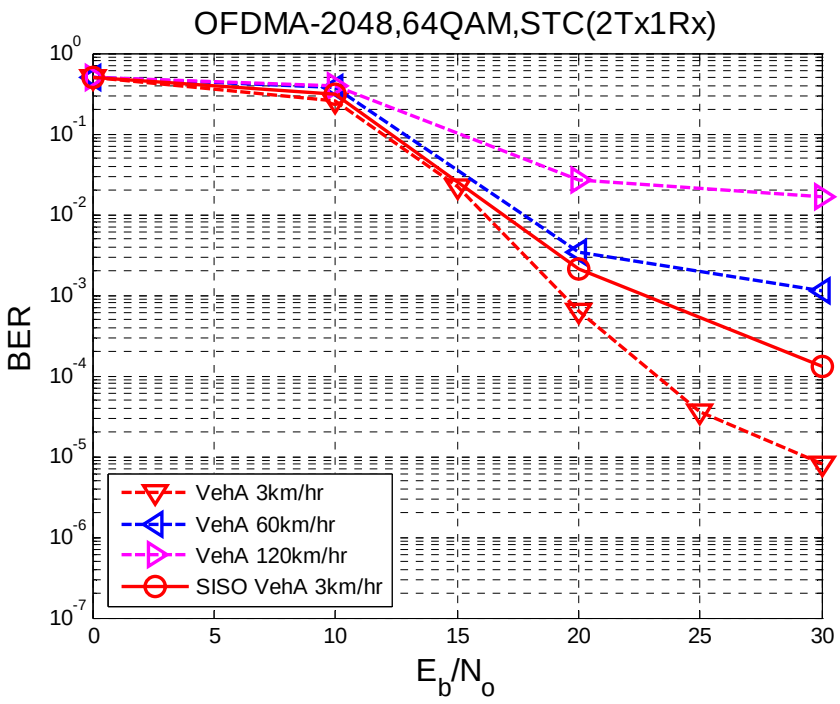

Figure 4.21: BER performance with STC (2Tx1Rx) and 64QAM in OFDMA-2048 mode under Veh A channel

Next, the performances of using AAS techniques are shown in Figures 4.22-4.27. Channel estimation is performed by using the pilot aided scheme. AAS techniques can generally be classified as either switched beamforming or adaptive beamforming. Because adaptive beamforming is generally more digital-processing intensive than switched beamforming, they tend to be more costly and complex. So switched beamforming is considered and simulated in this system. The transmitter is equipped with four antenna arrays and the receiver is equipped with one antenna. As seen in Figures 4.22, 4.24 and 4.26, AAS with 16 beams and 8 beams provide about 6 dB and 4 dB in performance gains under Vehicular A 3 km/hr channel environments. As the number of beams decreases, the radiation angle of each beam increases and the intended user may not be in the center of the main beam. As shown in Figures 4.23, 4.25 and 4.27, under Vehicular A 120 km/hr channel environments, it is obviously observed that the performance is poorer because the time-varying fading rate is so fast

that the weights computed over the preamble period are not suitable for the remaining symbols.

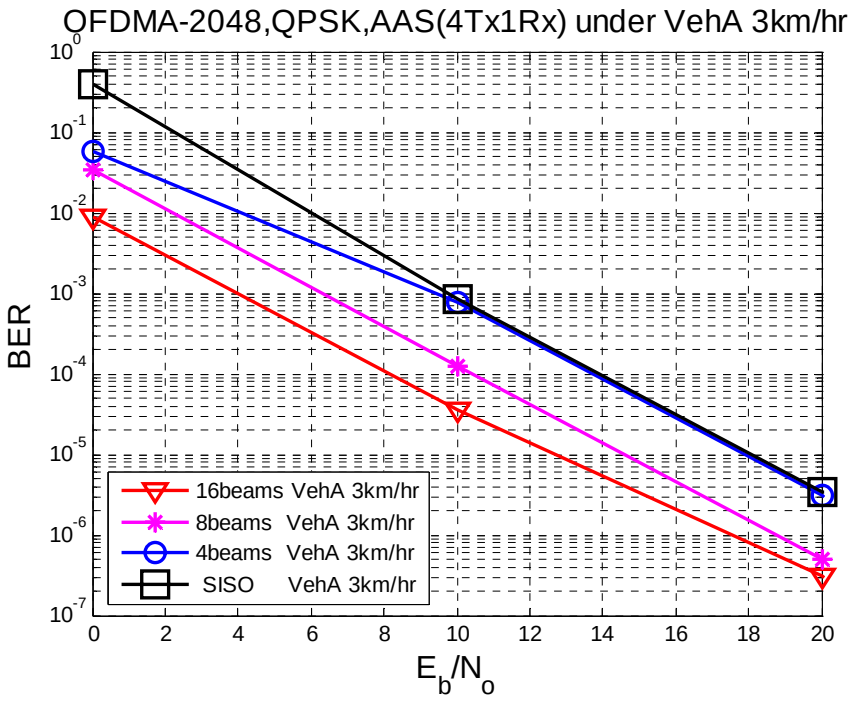

Figure 4.22: BER performance with AAS (4Tx1Rx) and QPSK in OFDMA-2048 mode under VehA 3 km/hr channel

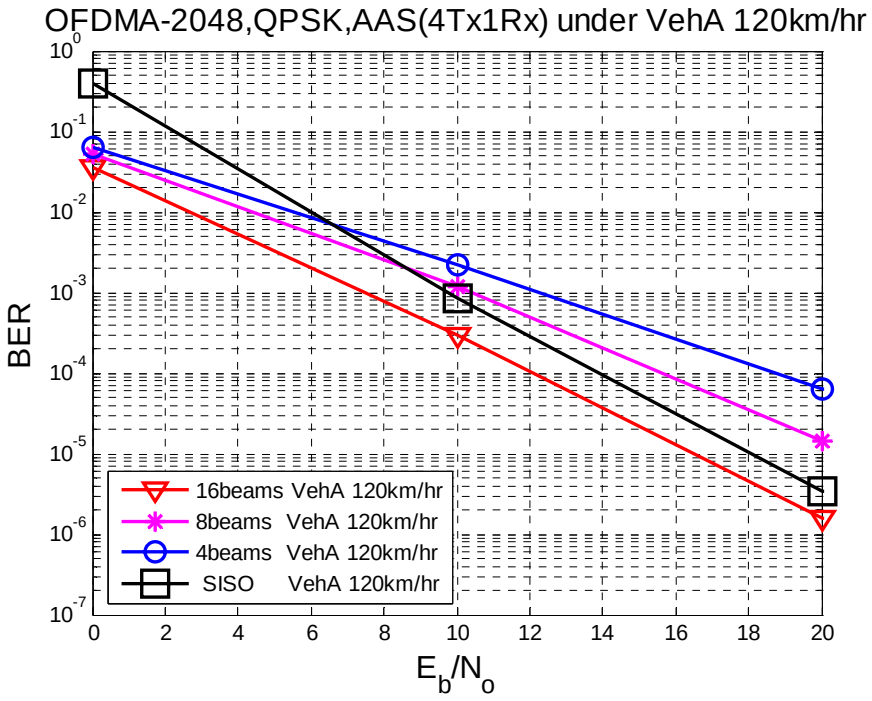

Figure 4.23: BER performance with AAS (4Tx1Rx) and QPSK in OFDMA-2048 mode under VehA 120 km/hr channel

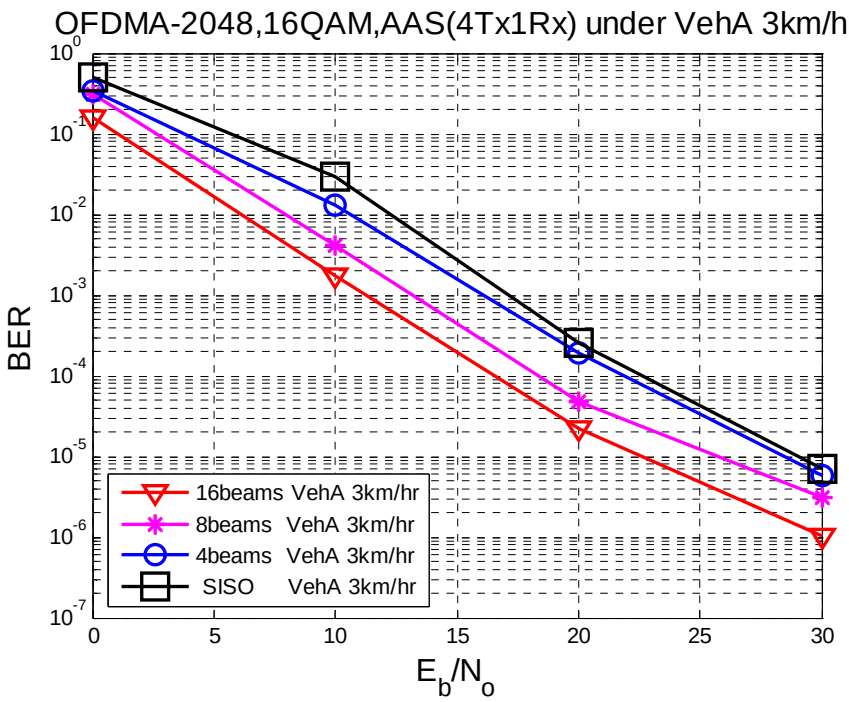

Figure 4.24: BER performance with AAS (4Tx1Rx) and 16QAM in OFDMA-2048 mode under VehA 3km/hr channel

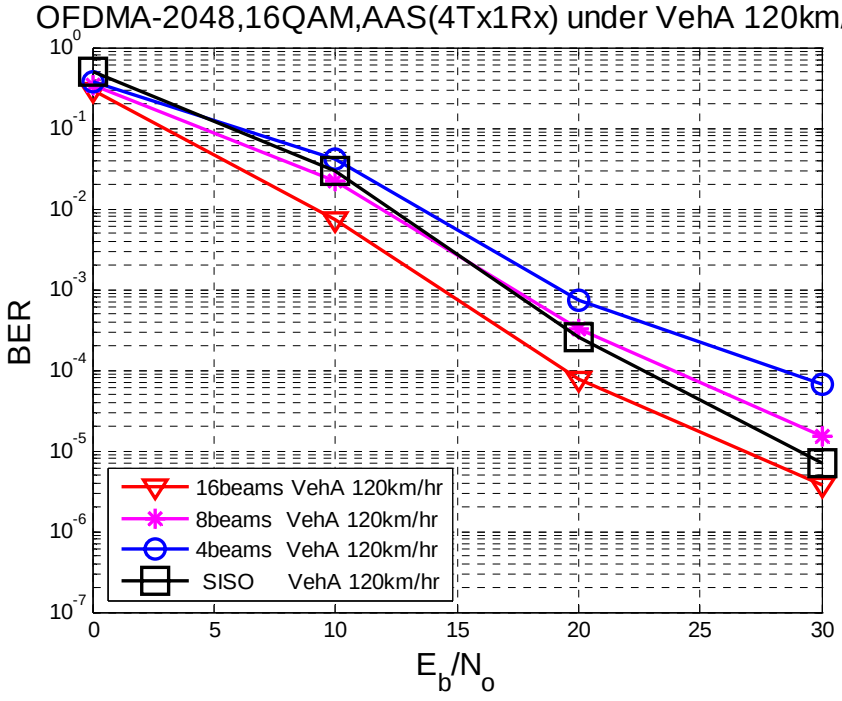

Figure 4.25: BER performance with AAS (4Tx1Rx) and 16QAM in OFDMA-2048 mode under VehA 120km/hr channel

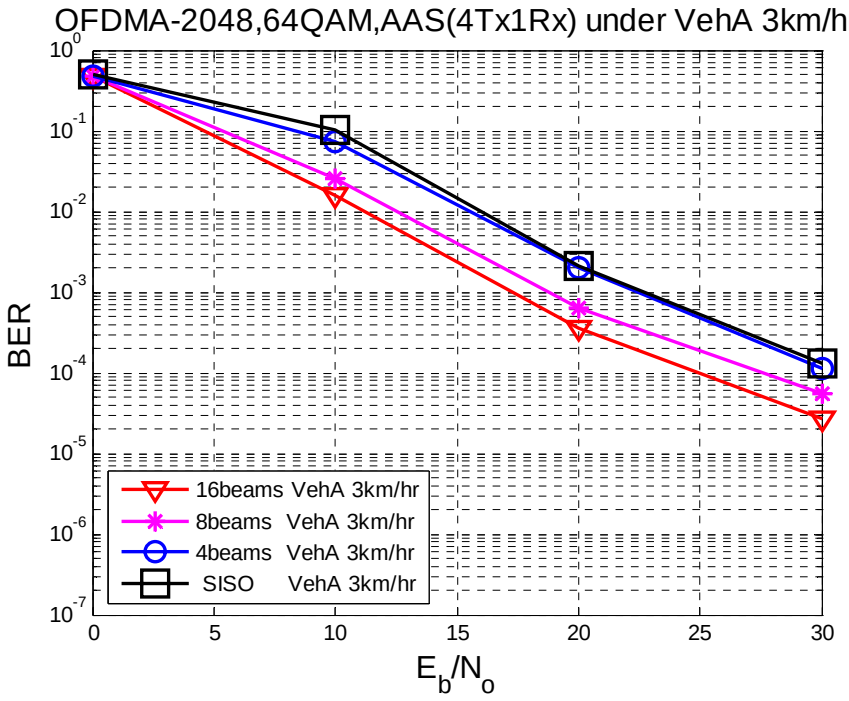

Figure 4.26: BER performance with AAS (4Tx1Rx) and 64QAM in OFDMA-2048 mode under VehA 3km/hr channel

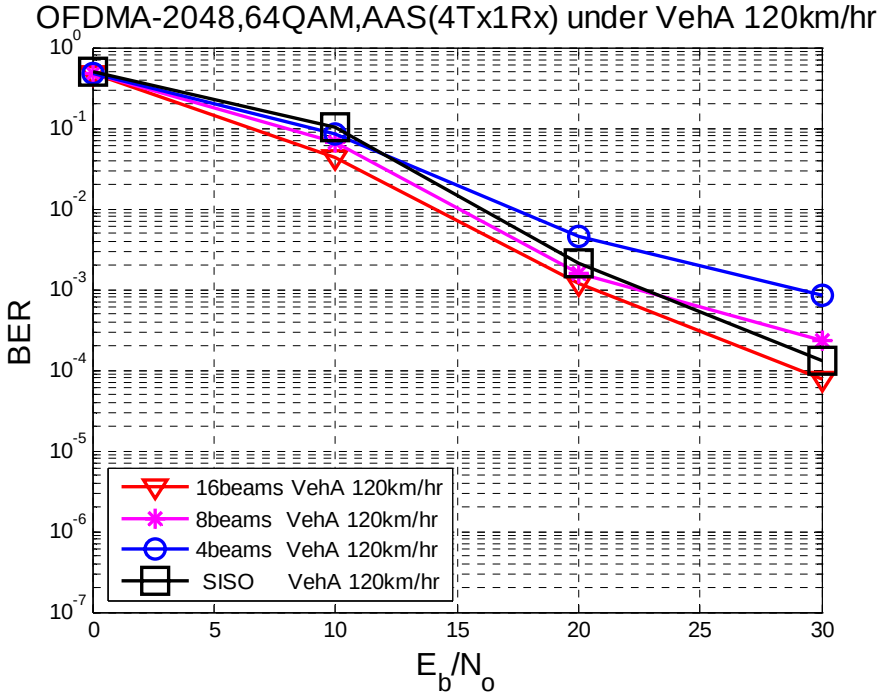

Figure 4.27: BER performance with AAS (4Tx1Rx) and 64QAM in OFDMA-2048 mode under Ve A 120km/hr channe

4.5 Summary

In this chapter, the proposed SC-OFDM-OFDMA SDR transmitter architecture is introduced first. We also introduce the procedures of determining the segmentation block size to fit the input data size of the encoder. At the receiver, the proposed SC-OFDM-OFDMA SDR receiver architecture via the concept of SDR is introduced. All the functional blocks have to be modified to adapt to the different air interfaces. Synchronization is first presented, which consists of the jointly designed timing and frequency synchronization algorithm. The jointly designed timing and frequency synchronization scheme proposed in Chapter 3 also needs to be modified to adapt to the different preamble structures. Then, channel estimation, phase estimation and residual frequency offset estimation are described in the rest of this chapter. After that, we highlight the multiple-antenna transmit techniques such as STC and AAS, implemented on the SDR system to gain the improved performances. Finally, we evaluate the performances of the joint design of SC-OFDM-OFDMA SDR system and confirm that it works reliably among the three modes.

Chapter 5

Conclusion

In this thesis, a jointly designed transceiver is developed for Single Carrier, OFDM and OFDMA under the SDR architecture. The jointly designed SC-OFDM-OFDMA SDR architecture is developed to support the various air-interface standards specified by IEEE 802.16-2005 on a single SDR platform. In this way, the system possesses as many common components as possible for these three modes, and the transmitter and receiver can be switched among the three modes via the operation of SDR concept.

In Chapter 2, the transmitter architecture and specification of IEEE 802.16-2005 WiMAX system have been introduced. In the rest of this chapter, we also introduce the multiple-antenna transmit techniques such as STC and AAS adopted in this system. In Chapter 3, we introduce two channel models: the first is the SUI channel model to form the fixed wireless channel environment and the second is the ITU channel model to form the mobile channel environment. After that, synchronization, channel estimation and phase estimation algorithms for this SDR system are established. In particular, we propose a jointly designed timing and frequency synchronization algorithm for the SDR architecture. The jointly designed timing and frequency synchronization scheme proposed can lower the computational complexity and obtain the reliable timing and

frequency offset estimates. We also use the phase estimators to perform residual frequency offset estimation. By this way, the residual frequency offset estimation scheme can co-work with the proposed jointly designed scheme to obtain a wider range and better accuracy of estimates.

In Chapter 4, we first review the concept of SDR. SDR technology facilitates the implementation of some of the functional modules by software in the MAC and PHY layers. This helps in building the reconfigurable software radio systems where dynamic selection of parameters for some software-defined functional modules is possible. Next, the transmitter and receiver architecture of the SC-OFDM-OFDMA SDR system are proposed. At the transmitter side, the data block size is determined by the FEC block, modulator, and the number of subchannels allocated. We describe three mathematical equations for the three modes to facilitate determining the uncoded data block size. At the receiver side, we focus on the three blocks such as timing and frequency synchronization block, channel estimation block, and phase estimation block. Although these algorithms have been mentioned in Chapter 3, they need to be modified to match the functions of the prescribed air interfaces by setting suitable parameters. In particular, the jointly designed timing and frequency synchronization scheme proposed is modified in accordance with different preamble structures: with short preamble and without short preamble. The simulations indicate the proposed timing and frequency synchronization scheme with the CP can work reliably and the performances are close to the ideal case as long as the CP length is long enough. After that, we generalize some results from the three modes and give the adjustable parameters for the three modes on the same SDR platform.

Finally, we study the multiple-antenna transmit techniques such as STC and AAS specified by IEEE 802.16-2005. Compared with the SISO transmission mode, STC transmit technique can improve the performance of the system significantly when the

SS is at low mobility. AAS can also obtain the improved performance through the use of more than one antenna elements at the BS. Both of the two transmit techniques have the same advantage of remaining only one antenna at the SS side. This key advantage can be utilized by increasing more cost and complexity only at the BS side without raising the complexity of user's devices.

Bibliography

[1] *IEEE Std 802.16e-2005 and IEEE Std 802.16-2004/Cor 1-2005*, "Part 16: air interface for fixed and mobile broadband wireless access systems," Feb. 2006.

[2] *IEEE Std 802.16-2004*, "Part 16: air interface for fixed broadband wireless access systems," Oct. 2004.

[3] "Mobile WiMAX - part 1: a technical overview and performance evaluation," *WiMAX Forum*, Feb. 2006.

[4] "Mobile WiMAX - part 2: a comparative analysis," *WiMAX Forum*, April 2006.

[5] John Hoadley and Al Javed, "Overview: technology innovation for wireless broadband access," *Nortel Technical Journal*, No. 2, July 2005.

[6] A. Salvekar, S. Sandhu, Q. Li, M. Vuong and X. Qian, "Multiple-antenna technology in WiMAX systems," *Intel Technology Journal*, Vol. 8, Aug.2004.

[7] S. Alamouti, "A simple transmit diversity technique for wireless communications," *IEEE Journal on Select Areas in Communications*, Vol. 16, No. 8, pp. 1451-1458, Oct. 1998.

[8] Jin M. Ku, Pil K. Kim, Se J. Lee, Simon Shin, and Chung G. Kang, "On the performance of broadband mobile internet access system," *ISWPC2006*, Jan. 2006.

[9] Shuenn Gi Lee, "Performance of concatenated FEC under fading channel in Wireless-MAN OFDM system," *Proceedings of the 19th International Conference on Advanced Information Networking and Applications*, July 2005.

[10] Pangan Ting, Yung-Yih Jian, Chia-Tsung Lin, Yu-Tao Hsieh, Chi-Fang Li, Tsan-Huang Chen, Shuenn Gi Lee, Wei Ping Chuang, Chao-Kai Wen and Racy J-H Cheng, "Downlink BER simulation for IEEE 802.16e OFDM-PHY," *Proceedings of 2005 International Symposium on Intelligent Signal Processing and Communication Systems*, June 2005.

[11] *IEEE 802.16a-03/01*, "Channel models for fixed wireless applications," June 2003.

[12] *Recommendation ITU-R M.1225*, "Guidelines for evaluation of radio transmission technologies for IMT-2000," 1997.

[13] P. Y Tsai, H. Y. Kang, and T. D. Chiueh, "Joint weighted least squares estimation of carrier-frequency offset and timing offset for OFDM systems over multipath fading channels," *IEEE Trans. Vehicular Technology*, Vol. 54, No. 1, Jan. 2005.

[14] D. K. Kim, S. H. Do, H. B. Cho, H. J. Choi,and K. B. Kim, "A new joint algorithm of symbol timing recovery and sampling clock adjustment for OFDM systems," *IEEE Trans. Consumer Electronics*, Vol. 44, No. 3, Aug. 1998.

[15] M. Wu and W. P. Zhu, "A preamble aided symbol and frequency synchronization scheme for OFDM systems," *Proceedings of IEEE International Symposium on Circuits and Systems*, pp. 2627-2630, Kobe, Japan, May 2005.

[16] Meng-Han Hsieh and Che-Ho Wei, "Channel estimation for OFDM systems based on comb-type pilot arrangement in frequency selective fading channels," *IEEE Trans. Consumer Electronics*, Vol. 44, pp. 217-225, Feb. 1998.

[17] B. Haberland, W. Koenig, A. Pascht, U. Weiss, "Software defined radio: a promising technology for multi-standard base stations," *Alcatel*, May 2005.

[18] Michael Komara, "SDR architecture ideally suited for evolving 802.16 WiMAX standards," *AirNet Communications*, Oct. 2004.

[19] Y. Shinagawa, "Software radio technologies," *1st int'l. SW Radio Wksp.*, Rhodes, Greece, June 1998.

[20] E. Buracchini, "The software radio concept," *IEEE Commun. Mag.*, vol. 38, no. 9, pp. 138-143, Sept. 2000.

[21] J. Mitola, "The software radio architecture," *IEEE Commun. Mag.*, vol. 33, no. 5, pp. 26-38, May 1995.

[22] A. N. Mody and G. L. Stuber, "Synchronization for MIMO OFDM systems," School of Electrical and Computer Engineering, Georgia Institute of Technology, Atlanta..

[23] R. Van Nee and R. Prasad, *OFDM for Wireless Multimedia Communications*, Artech House, 1999.

[24] J. G. Proakis, *Digital Communications*, 4th edition, McGraw-Hill, 2001.

[25] S. J. Yang, Y. C. Lei, T. D. Chiueh, “Design and simulation of a baseband transceiver for IEEE 802.16a OFDM-Mode subscriber stations,” *IEEE Asia-Pacific Conference on Circuit and Systems*, Dec. 2004.

[26] P. H. Moose, “A technique for orthogonal frequency division multiplexing frequency offset correction,” *IEEE Trans. Commun.*, Vol. 42, pp. 2908-2914, Oct. 1994.

[27] S. A. Fechtel, “OFDM carrier and sampling frequency synchronization and its performnance on stationary and mobile channels,” *IEEE Trans. Consumer Electronics*, Vol. 46, No. 3, pp. 438-441, Aug. 2000.

[28] M. Speth, S. A. Fechtel, G. Fock and H. Meyr, “Optimum receiver design for OFDM-based broadband transmission part II: a case study,” *IEEE Trans. Commun*., Vol. 44, No. 4, pp. 571-578, Apr. 2001.